MIMO Capacity Characterization for Movable Antenna Systems

Wenyan Ma, *Student Member, IEEE*, Lipeng Zhu, *Member, IEEE*, and Rui Zhang, *Fellow, IEEE*

***Abstract*—In this paper, we propose a new multiple-input multiple-output (MIMO) communication system with movable antennas (MAs) to exploit the antenna position optimization for enhancing the capacity. Different from conventional MIMO systems with fixed-position antennas (FPAs), the proposed system can flexibly change the positions of transmit/receive MAs, such that the MIMO channel between them is reconfigured to achieve higher capacity. We aim to characterize the capacity of MA-enabled point-to-point MIMO communication systems, by jointly optimizing the positions of transmit and receive MAs as well as the covariance of transmit signals. First, we develop an efficient alternating optimization algorithm to find a locally optimal solution by iteratively optimizing the transmit covariance matrix and the position of each transmit/receive MA with the other variables being fixed. Next, we propose alternative algorithms of lower complexity for capacity maximization in the low-SNR regime and for the multiple-input single-output (MISO) and single-input multiple-output (SIMO) cases. Numerical results show that our proposed MA systems significantly improve the MIMO channel capacity compared to traditional FPA systems as well as various benchmark schemes, and useful insights are drawn into the capacity gains of MA systems.**

***Index Terms*—Capacity, multiple-input multiple-output (MIMO), movable antenna (MA), alternating optimization.**

I. Introduction

The proliferation of wireless applications, including high-quality video streaming and augmented/virtual reality (AR/VR), has spurred the need for elevated capacity in next-generation wireless communication systems. To achieve this goal, multiple-input multiple-output (MIMO) and massive MIMO communications have been the key enabling technologies [2], [3]. However, although MIMO/massive MIMO can enhance the wireless channel capacity and system spectral efficiency significantly, they generally demand considerably higher hardware costs and energy consumption, due to the growing number of radio frequency (RF) chains and/or antennas required for wireless systems operating at higher frequency bands [4], [5].

To reduce the number of RF chains, antenna selection (AS) is a practical solution for capturing a large portion of the channel capacity in MIMO systems by properly selecting a small number of antennas with favorable channels from the a large candidate set [6], [7]. However, deploying more candidate antennas requires higher hardware cost, and the overhead of channel estimation and the computational complexity of AS algorithms grow greatly with the total number of antennas [8]. To further exploit the array gain with a small number of RF chains, different antenna architectures have been proposed to maximize the achievable rate of communication systems by properly designing the analog/hybrid precoding/combining matrix [9]–[12]. By optimizing the diagonal power allocation matrix and analog precoding (AP) matrix at the transmitter as well as the analog combining matrix at the receiver, the channel capacity can be improved compared with that of AS systems for fading channels [9]. Moreover, the hybrid digital-analog precoding architecture was studied in [10]. By designing the hybrid precoding (HP) matrix based on instantaneous channel state information (CSI), the HP system outperforms the AP system and fully digital (FD) system in terms of energy efficiency. Furthermore, the multiuser interference channel was considered in [11], [12]. By controlling the on-off state of all phase shifters (PSs) and RF chains through a switch network, the energy efficiency of multiple users can be improved [11]. Besides, the PS-antenna connection network and PSs were jointly designed to maximize the users' average downlink achievable rate [12]. However, since the antennas are deployed at fixed positions in conventional MIMO/massive MIMO with/without AS or HP, they cannot fully utilize the spatial variation of wireless channels in a given transmit/receive region, especially with a limited number of antennas.

To improve the channel capacity under the fixed array structure, the rotatable uniform linear array (RULA) was proposed by mechanically rotating the transmit/receive array to achieve better channel conditions [13], [14]. However, since the transmit/receive array can only be reconfigured by rotation, the spatial channel variation cannot be fully exploited. To further explore the degrees of freedom (DoFs) in the spatial domain for improving the communication performance, the fluid antenna system (FAS) was proposed by changing the antenna position flexibly over a one-dimensional (1D) line [15], [16]. By using conductive fluids as materials for antennas, the position of a receive antenna can be switched freely among all candidate ports over a fixed-length line, and thus the signal with the highest signal-to-noise ratio (SNR) can be received [15]. By setting the number of possible positions large enough, a single-antenna FAS can even achieve lower outage probability compared to multiple-antenna systems with maximum ratio combining (MRC). Moreover, the fluid antenna multiple access (FAMA) was studied in [16] to support multiple transceivers with a single fluid antenna at each mobile user. By selecting the positions of the fluid

This work is supported in part by Ministry of Education, Singapore under Award T2EP50120-0024, Advanced Research and Technology Innovation Centre (ARTIC) of National University of Singapore under Research Grant R-261-518-005-720, and The Guangdong Provincial Key Laboratory of Big Data Computing. An earlier version of this paper was presented in part at the IEEE International Conference on Communications (ICC), Rome, Italy, 2023 [1]. The associate editor coordinating the review of this article and approving it for publication was M. Wang. *(Corresponding author: Lipeng Zhu.)*

W. Ma and L. Zhu are with the Department of Electrical and Computer Engineering, National University of Singapore, Singapore 117583 (Email: wenyan@u.nus.edu, zhulp@nus.edu.sg).

R. Zhang is with School of Science and Engineering, Shenzhen Research Institute of Big Data, The Chinese University of Hong Kong, Shenzhen, Guangdong 518172, China (e-mail: rzhang@cuhk.edu.cn). He is also with the Department of Electrical and Computer Engineering, National University of Singapore, Singapore 117583 (e-mail: elezhang@nus.edu.sg).

antennas at different users, the favorable channel condition with mitigated interference can be obtained, thereby achieving a significant capacity gain. It was shown in [15], [16] that changing the positions of antennas can efficiently improve the wireless channel capacity. However, due to the limitations of liquid materials, the FAS can only support a single fluid antenna moving over a 1D line, which limits its capability for fully exploiting the wireless channel variation in the spatial domain.

To fully explore the ultimate capacity of MIMO systems, the concept of continuous-aperture MIMO (CAP-MIMO) was proposed [17], which is also called holographic MIMO [18], [19], large intelligent surface [20], or holographic surface [21], [22]. By deploying a large number of sub-wavelength radiation elements in a compact surface, CAP-MIMO can be regarded as a quasi-continuous electromagnetic surface with controllable current density. Although the recent advance in highly-flexible programmable meta-materials has made the CAP-MIMO more practically implementable, some critical challenges still remain unsolved [18], such as the efficient estimation of ultra high-dimensional CAP-MIMO channels and the efficient current density optimization subject to a large number of practical constraints.

To exploit more spatial DoFs for enhancing the channel capacity, we propose a new MIMO communication system enabled by movable antennas (MAs). Specifically, by connecting the MAs to RF chains via flexible cables, the positions of MAs can be adjusted by controllers in real time, such as stepper motors or servos [23]–[25]. Different from conventional MIMO systems with fixed-position antennas (FPAs), the proposed system can flexibly change the positions of transmit/receive MAs, such that the MIMO channel matrix between them can be reshaped for achieving higher capacity. For MIMO systems, we can jointly optimize the positions of transmit and receive MAs for the channel capacity maximization. To achieve high channel capacity in MIMO systems, it is common to transmit multiple data streams simultaneously. To maximize the channel capacity, the positions of transmit and receive MAs must be optimized to balance the channel gains for each of the spatial data streams.

Existing studies have validated the great potentials of MA-enabled wireless communications [1], [26]–[28]. In [26], the overview of the promising applications for MA-aided wireless communications was provided. It was shown that employing MAs can improve the communication performance in terms of signal power improvement, interference mitigation, flexible beamforming, and spatial multiplexing. Besides, the field-response-based channel model and MA architecture were proposed for the single-MA system in [27], where the SNR gain over its FPA counterpart was investigated under both deterministic and stochastic channels. In [1], an MA-enabled MIMO communication system was considered, where the receive MAs' positioning and transmit covariance matrix were jointly optimized for maximizing the channel capacity. It was revealed that the optimization of the receive MAs' positions can reshape the MIMO channel matrix into a more favorable condition for capacity maximization. Moreover, the MA-enabled multiuser communication system was considered in [28], where the MAs' positions of multiple users were jointly optimized to minimize the total transmit power, subject to the minimum achievable rate requirement of each user. It was revealed that the antenna position optimization can significantly decrease the total transmit power of users as compared to conventional FPA systems. Note that the proposed MA-enabled communication system is different from conventional AS systems. On one hand, the AS systems can only deploy a finite number of antennas in discrete antenna ports, which cannot fully exploit the channel spatial variation over all locations near the Tx/Rx. In comparison, each MA can be flexibly moved in a continuous region around the Tx/Rx and thus attain improved diversity/multiplexing performance. On the other hand, the performance of MA systems can be improved by simply enlarging the size of the region for antenna moving. However, for approaching the performance of MA systems, the AS systems need to deploy more antennas to cover the same region, which result in more substantial hardware cost. Although the AS algorithm can be applied for MA systems by quantizing the transmit/receive area into discrete locations and constraining each MA to move over them only, the computational complexity for exhaustively searching the antenna positions for MAs increases significantly with the size of transmit/receive area, especially when the number of MAs increases. Thus, more efficient MA position optimization algorithms should be investigated to reduce the computational complexity of exhaustive search.

In this paper, we study the joint optimization of the transmit and receive MAs' positions as well as the transmit signals' covariance matrix to maximize the capacity of the MA-enabled point-to-point MIMO system, with MAs equipped at both the transmitter and receiver. To characterize the fundamental capacity limit, we assume that perfect CSI is available at both the transmitter and receiver. The main contributions of this paper are summarized as follows:

- Firstly, we derive the capacity maximization problem for the MA-enabled MIMO communication systems, which is non-convex and thus difficult to be optimally solved. To tackle this problem efficiently, we propose an alternating optimization algorithm by iteratively optimizing the transmit covariance matrix and the position of each transmit/receive MAs with the other variables being fixed. In particular, given the transmit covariance matrix, we leverage the convex relaxation technique to obtain a locally optimal solution for the transmit/receive MA-positioning optimization subproblem. It is shown that the proposed algorithm converges to a suboptimal solution at least.
- Moreover, we investigate the MA-enabled MIMO channel capacity in the low-SNR regime, and propose an alternative algorithm for solving the capacity maximization problem with lower complexity. In addition, we further simplify the proposed algorithm for the capacity maximization in the special cases of multiple-input single-output (MISO) and single-input multiple-output (SIMO) channels with MAs.
- Finally, we present sufficient numerical results to demon-

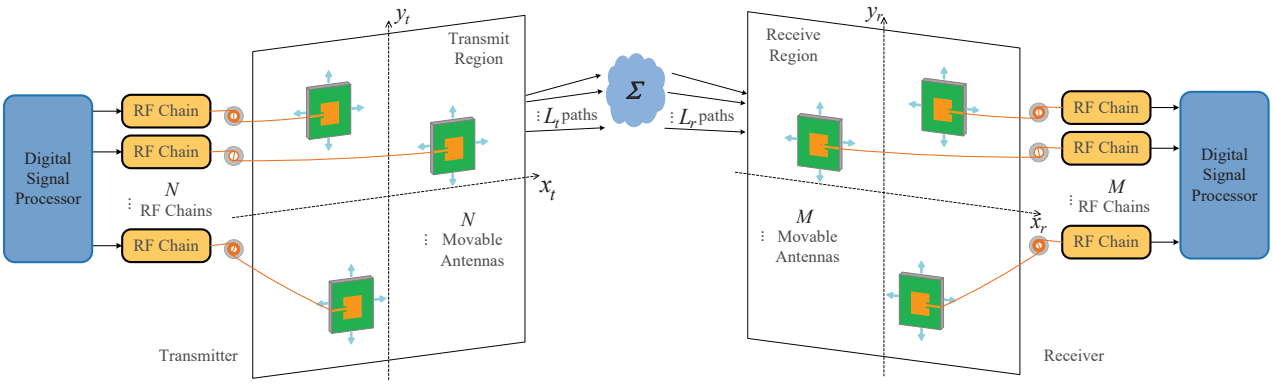

Fig. 1. The MA-enabled MIMO communication system.

strate the capacity gains of the proposed MA-enabled MIMO systems over conventional MIMO systems with FPAs, and shed more light on the performance gains of MA systems. In particular, it is shown that by jointly designing the positions of transmit and receive MAs, the total MIMO channel power can undergo significant improvement while the condition number of the MIMO channel decreases with the size of the transmit/receive region, thus leading to higher MIMO channel capacity.

The remainder of this paper is organized as follows. Section II describes the system model and the problem formulation to characterize the MA-enabled MIMO system capacity. In Section III, we propose an alternating optimization algorithm to solve the formulated problem under different setups. Section IV provides numerical results and discussions. Finally, we conclude this paper in Section V.

Notations: Symbols for vectors (lower case) and matrices (upper case) are in boldface. $(\cdot)^T$ and $(\cdot)^H$ denote the transpose and conjugate transpose (Hermitian), respectively. The set of $P \times Q$ dimensional complex and real matrices is denoted by $\mathbb{C}^{P\times Q}$ and $\mathbb{R}^{P\times Q}$, respectively. We use $\boldsymbol{a}[p]$ and $\boldsymbol{A}[p,q]$ to denote the pth entry of vector $\boldsymbol{a}$ and the entry of matrix $\boldsymbol{A}$ in its pth row and qth column, respectively. $\mathrm{Re}\{\boldsymbol{a}\}$ denotes the real part of vector $\boldsymbol{a}$. The trace of matrix $\boldsymbol{A}$ is denoted by $\mathrm{Tr}(\boldsymbol{A})$. $\mathrm{diag}(\boldsymbol{a})$ denotes a square diagonal matrix with the elements of vector $\boldsymbol{a}$ on the main diagonal, while $\mathrm{diag}(\boldsymbol{A})$ denotes a column vector consisting of the main diagonal elements of matrix $\boldsymbol{A}$. $\boldsymbol{A} \succeq 0$ indicates that $\boldsymbol{A}$ is a positive semi-definite matrix. $\mathcal{CN}(0,\boldsymbol{\Gamma})$ denotes the circularly symmetric complex Gaussian (CSCG) distribution with mean zero and covariance matrix $\boldsymbol{\Gamma}$. We use $\boldsymbol{I}_K$ to represent the identity matrix of order K. The 2-norm of vector $\boldsymbol{a}$ is denoted by $\|\boldsymbol{a}\|_2$. $\|\boldsymbol{A}\|_2$ and $\|\boldsymbol{A}\|_F$ denote the spectral norm and Frobenius norm of matrix $\boldsymbol{A}$, respectively. $\mathrm{rank}(\boldsymbol{A})$ denotes the rank of matrix $\boldsymbol{A}$. The amplitude and phase of complex number a are denoted by $|a|$ and $\angle a$, respectively.

II. System Model and Problem Formulation

A. MA-Enabled MIMO System

As shown in Fig. 1, we consider a MIMO communication system with N transmit MAs and M receive MAs. The transmit and receive MAs are connected to RF chains via flexible cables, and thus their positions can be adjusted in real time. The positions of the nth ($n = 1, 2, \ldots, N$) transmit MA and mth ($m = 1, 2, \ldots, M$) receive MA can be represented by Cartesian coordinates $\boldsymbol{t}_n = [x_{t,n}, y_{t,n}]^T \in \mathcal{C}_t$ and $\boldsymbol{r}_m = [x_{r,m}, y_{r,m}]^T \in \mathcal{C}_r$, where $\mathcal{C}_t$ and $\mathcal{C}_r$ denote the given two-dimensional (2D) regions within which the transmit and receive MAs can move freely, respectively. Without loss of generality, we set $\mathcal{C}_t$ and $\mathcal{C}_r$ as square regions with size $A \times A$.

We consider narrow-band quasi-static channels, where the transmitter and receiver are static or move slowly in the given regions. In contrast, the transmit and receive MAs are assumed to be able to move sufficiently fast, such that the time overhead for adjusting MA positions is tolerable compared to the much longer channel coherence time. For MA-enabled MIMO communication systems, the channel is reconfigurable by adjusting the positions of transmit and receive MAs. Denote the collections of the coordinates of N transmit MAs and M receive MAs by $\tilde{\boldsymbol{t}} = [\boldsymbol{t}_1, \boldsymbol{t}_2, \ldots, \boldsymbol{t}_N] \in \mathbb{R}^{2\times N}$ and $\tilde{\boldsymbol{r}} = [\boldsymbol{r}_1, \boldsymbol{r}_2, \ldots, \boldsymbol{r}_M] \in \mathbb{R}^{2\times M}$, respectively. Then, the MIMO channel matrix from the transmitter to the receiver is given by $\boldsymbol{H}(\tilde{\boldsymbol{t}}, \tilde{\boldsymbol{r}}) \in \mathbb{C}^{M\times N}$, which is a function of $\tilde{\boldsymbol{t}}$ and $\tilde{\boldsymbol{r}}$ in general.

Let $\boldsymbol{s} \in \mathbb{C}^N$ denote the transmit signal vector. The corresponding covariance matrix is defined as $\boldsymbol{Q} \triangleq \mathbb{E}\{\boldsymbol{s}\boldsymbol{s}^H\} \in \mathbb{C}^{N\times N}$, with $\boldsymbol{Q} \succeq \boldsymbol{0}$. We consider an average sum power constraint at the transmitter given by $\mathbb{E}\{\|\boldsymbol{s}\|_2^2\} \le P$, which is equivalent to $\mathrm{Tr}(\boldsymbol{Q}) \le P$. The received signal vector is thus given by

$$\boldsymbol{y}(\tilde{\boldsymbol{t}}, \tilde{\boldsymbol{r}}) = \boldsymbol{H}(\tilde{\boldsymbol{t}}, \tilde{\boldsymbol{r}})\boldsymbol{s} + \boldsymbol{z}, \tag{1}$$

where $\boldsymbol{z} \sim \mathcal{CN}(0, \sigma^2 \boldsymbol{I}_M)$ denotes the additive white Gaussian noise (AWGN) vector at the receiver, which is assumed to be CSCG distributed with zero mean, and σ^2 being the average noise power.

B. Field-Response Based Channel Model

For the MA-enabled MIMO communication system, the channel matrix is determined by the signal propagation environment and the positions of transmit and receive MAs. We consider the far-field wireless channel model, where the size of the transmit/receive region is much smaller than the signal propagation distance [27], [28]. Thus, for each channel path

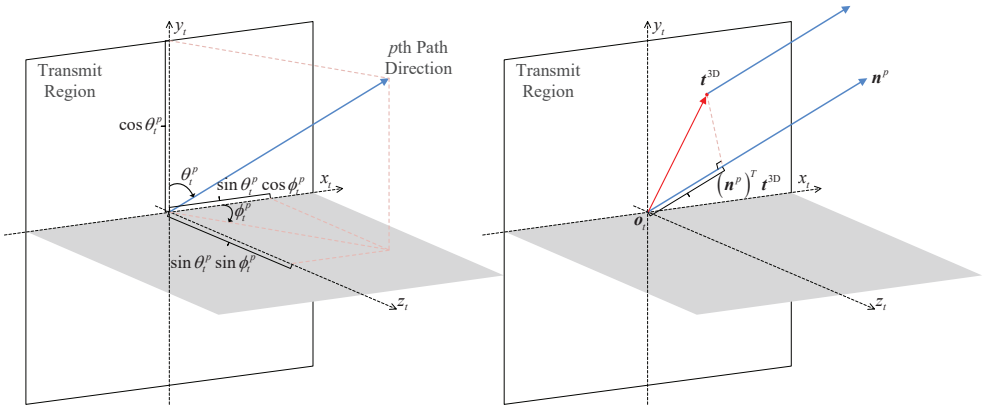

Fig. 2. The spatial angles and path differences for transmit region.

component, all MAs in the transmit/receive region experience the same angle of departure (AoD)/angle of arrival (AoA), and amplitude of the complex path coefficient [1], while the phase of the complex path coefficient varies for different transmit/receive MAs at different positions.

Denote the number of transmit paths and receive paths as L_t and L_r, respectively. As shown in Fig. 2, the elevation and azimuth AoDs of the pth ($p = 1, 2, \ldots, L_t$) transmit path are denoted by $\theta_t^p \in [0, \pi]$ and $\phi_t^p \in [0, \pi]$, respectively. Then, the normalized wave vector of the pth transmit path can be represented by $\boldsymbol{n}^p = [\sin\theta_t^p \cos\phi_t^p, \cos\theta_t^p, \sin\theta_t^p \sin\phi_t^p]^T$. Denote the three-dimensional (3D) coordinate vector of the transmit MA and origin of the transmit region by $\boldsymbol{t}^{\rm 3D} = [x_t, y_t, 0]^T$ and $\boldsymbol{o}_t = [0, 0, 0]^T$, respectively. Then, the difference of the signal propagation for the pth transmit path between position $\boldsymbol{t}^{\rm 3D}$ and $\boldsymbol{o}_t$ is given by

$$\rho_t^p(\boldsymbol{t}) = (\boldsymbol{n}^p)^T(\boldsymbol{t}^{\rm 3D} - \boldsymbol{o}_t) = x_t \sin\theta_t^p \cos\phi_t^p + y_t \cos\theta_t^p. \quad (2)$$

Thus, the phase difference of the pth transmit path between $\boldsymbol{t}^{\rm 3D}$ and $\boldsymbol{o}_t$ is $2\pi\rho_t^p(\boldsymbol{t})/\lambda$, where λ is the carrier wavelength. The field response vector of the transmit MA can be defined as

$$\boldsymbol{g}(\boldsymbol{t}) \triangleq \left[e^{j\frac{2\pi}{\lambda}\rho_t^1(\boldsymbol{t})}, e^{j\frac{2\pi}{\lambda}\rho_t^2(\boldsymbol{t})}, \ldots, e^{j\frac{2\pi}{\lambda}\rho_t^{L_t}(\boldsymbol{t})}\right]^T \in \mathbb{C}^{L_t}. \quad (3)$$

By stacking $\boldsymbol{g}(\boldsymbol{t}_n)$ of all N transmit MAs, the field response matrix of all the N transmit MAs is given by

$$\boldsymbol{G}(\tilde{\boldsymbol{t}}) \triangleq [\boldsymbol{g}(\boldsymbol{t}_1), \boldsymbol{g}(\boldsymbol{t}_2), \ldots, \boldsymbol{g}(\boldsymbol{t}_N)] \in \mathbb{C}^{L_t \times N}. \quad (4)$$

Similarly, denote the elevation and azimuth AoAs of the qth ($q = 1, 2, \ldots, L_r$) receive path as $\theta_r^q \in [0, \pi]$ and $\phi_r^q \in [0, \pi]$, respectively. The field response vector of the receive MA is defined as

$$\boldsymbol{f}(\boldsymbol{r}) \triangleq \left[e^{j\frac{2\pi}{\lambda}\rho_r^1(\boldsymbol{r})}, e^{j\frac{2\pi}{\lambda}\rho_r^2(\boldsymbol{r})}, \ldots, e^{j\frac{2\pi}{\lambda}\rho_r^{L_r}(\boldsymbol{r})}\right]^T \in \mathbb{C}^{L_r}, \quad (5)$$

where $\rho_r^q(\boldsymbol{r}) = x_r \sin\theta_r^q \cos\phi_r^q + y_r \cos\theta_r^q$ is the difference of the signal propagation distance for the qth receive path between position $\boldsymbol{r}$ and the origin of the receive region. Thus, the field response matrix of all the M receive MAs is written as

$$\boldsymbol{F}(\tilde{\boldsymbol{r}}) \triangleq [\boldsymbol{f}(\boldsymbol{r}_1), \boldsymbol{f}(\boldsymbol{r}_2), \ldots, \boldsymbol{f}(\boldsymbol{r}_M)] \in \mathbb{C}^{L_r \times M}. \quad (6)$$

Furthermore, we define the path response matrix from the origin of the transmit region to that of the receive region as $\boldsymbol{\Sigma} \in \mathbb{C}^{L_r \times L_t}$, where $\boldsymbol{\Sigma}[q, p]$ is the response between the pth transmit path and the qth receive path. As a result, the channel matrix from the transmitter to the receiver is given by

$$\boldsymbol{H}(\tilde{\boldsymbol{t}}, \tilde{\boldsymbol{r}}) = \boldsymbol{F}(\tilde{\boldsymbol{r}})^H \boldsymbol{\Sigma} \boldsymbol{G}(\tilde{\boldsymbol{t}}). \quad (7)$$

C. Problem Formulation

To investigate the theoretical capacity limit of the MA-enabled MIMO communication system, the perfect multi-path channel components are assumed to be available. Thus, the MIMO channel capacity can be written as [2] [3]

$$C(\tilde{\boldsymbol{t}}, \tilde{\boldsymbol{r}}) = \max_{\substack{\boldsymbol{Q}:\boldsymbol{Q}\succeq\boldsymbol{0}, \\ {\rm Tr}(\boldsymbol{Q})\le P}} \log_2 \det\left(\boldsymbol{I}_M + \frac{1}{\sigma^2}\boldsymbol{H}(\tilde{\boldsymbol{t}}, \tilde{\boldsymbol{r}})\boldsymbol{Q}\boldsymbol{H}(\tilde{\boldsymbol{t}}, \tilde{\boldsymbol{r}})^H\right). \quad (8)$$

Note that different from the conventional MIMO channel with FPAs, the MA-enabled MIMO channel capacity shown in (8) is depended on the positions of transmit and receive MAs $\tilde{\boldsymbol{t}}$ and $\tilde{\boldsymbol{r}}$, which influence the channel matrix $\boldsymbol{H}(\tilde{\boldsymbol{t}}, \tilde{\boldsymbol{r}})$ as well as the corresponding optimal transmit covariance matrix $\boldsymbol{Q}$.

[1]To characterize the theoretical performance limit of the MA-enabled MIMO communication system, the multi-path channel components between $\mathcal{C}_t$ and $\mathcal{C}_r$ are assumed to be known for optimization in this paper. To acquire the information of such multi-path channel components, MAs can be moved to a sufficient number of locations for channel measurement. Based on the channel measurements, sparse signal recovery algorithms, such as compressed sensing (CS), can be employed to estimate the multi-path channel components such as the AoDs, AoAs, and path coefficients of different paths [29].

[2]If the optimal solution for the positions of transmit and receive MAs is derived, we can obtain the maximum capacity for MA-enabled MIMO systems. While for any locally optimal position solution, $C(\tilde{\boldsymbol{t}}, \tilde{\boldsymbol{r}})$ represents the MIMO capacity for the given MA positions. Thus, we use the term "capacity" throughout this paper for consistency.

[3]In this paper, we focus on characterizing the point-to-point MIMO communication system capacity without co-channel interference. Nonetheless, another parallel work [28] has recently shown that the interference among multiple users can also be efficiently mitigated by optimizing the MAs' positions.

In order to avoid the coupling effect between the antennas in the transmit/receive region, a minimum distance D is required between each pair of antennas, i.e., $\|\boldsymbol{t}_k-\boldsymbol{t}_l\|_2\geq D$, $k,l=1,2,\ldots,N$, $k\neq l$, and $\|\boldsymbol{r}_k-\boldsymbol{r}_l\|_2\geq D$, $k,l=1,2,\ldots,M$, $k\neq l$. Then, we aim to maximize the capacity of an MA-enabled MIMO channel by jointly optimizing the MA positions $\tilde{\boldsymbol{t}}$, $\tilde{\boldsymbol{r}}$ and the transmit signals' covariance matrix $\boldsymbol{Q}$, subject to the minimum distance requirements for the MA positions. Accordingly, we formulate the optimization problem as

$$\text{(P1)}\quad \max_{\tilde{\boldsymbol{t}},\tilde{\boldsymbol{r}},\boldsymbol{Q}}\quad \log_2\det\left(\boldsymbol{I}_M+\frac{1}{\sigma^2}\boldsymbol{H}(\tilde{\boldsymbol{t}},\tilde{\boldsymbol{r}})\boldsymbol{Q}\boldsymbol{H}(\tilde{\boldsymbol{t}},\tilde{\boldsymbol{r}})^H\right) \tag{9a}$$

$$\text{s.t.}\quad \tilde{\boldsymbol{t}}\in\mathcal{C}_t, \tag{9b}$$

$$\tilde{\boldsymbol{r}}\in\mathcal{C}_r, \tag{9c}$$

$$\|\boldsymbol{t}_k-\boldsymbol{t}_l\|_2\geq D,\quad k,l=1,2,\ldots,N,\quad k\neq l, \tag{9d}$$

$$\|\boldsymbol{r}_k-\boldsymbol{r}_l\|_2\geq D,\quad k,l=1,2,\ldots,M,\quad k\neq l, \tag{9e}$$

$$\mathrm{Tr}(\boldsymbol{Q})\leq P, \tag{9f}$$

$$\boldsymbol{Q}\succeq\boldsymbol{0}. \tag{9g}$$

Problem (P1) is difficult to solve because the objective function is highly non-concave with respect to the MA positions $\tilde{\boldsymbol{t}}$ and $\tilde{\boldsymbol{r}}$, and the minimum distance constraints in (9d) and (9e) are non-convex. Besides, the coupling between $\boldsymbol{Q}$, $\tilde{\boldsymbol{t}}$, and $\tilde{\boldsymbol{r}}$ makes (P1) more intractable.

III. Proposed Algorithm

In this section, we present an alternating optimization algorithm to solve (P1). First, (P1) is transferred into a more tractable form with respect to $\{\boldsymbol{t}_n\}_{n=1}^N\cup\{\boldsymbol{r}_m\}_{m=1}^M\cup\boldsymbol{Q}$. Then, three subproblems are solved in the sequel, which respectively optimize the transmit signals' covariance matrix $\boldsymbol{Q}$, one transmit MA position $\boldsymbol{t}_n$, and one receive MA position $\boldsymbol{r}_m$, with all the other variables being fixed. The developed alternating optimization algorithm can obtain a (at least) locally optimal solution for (P1) by iteratively solving the above three subproblems in an alternate manner. After that, by deriving more manageable expressions for the MIMO channel capacity in the low-SNR regime, we present an alternative solution for (P1) with lower complexity. Finally, we investigate specific cases of (P1) that involve a single MA either at the transmitter or at the receiver, i.e., the SIMO/MISO setup, and propose simplified algorithms for them.

A. Alternating Optimization for (P1)

In this subsection, we present the framework of the proposed alternating optimization method to address (P1). The primary concept involves the iterative resolution of a sequence of subproblems derived from (P1), with each subproblem focusing on the optimization of a single variable in the set $\{\boldsymbol{t}_n\}_{n=1}^N\cup\{\boldsymbol{r}_m\}_{m=1}^M\cup\boldsymbol{Q}$ with the remaining $M+N$ variables fixed, which tackles the main difficulty of the complicated coupling among the optimization variables.

1) Optimization of $\boldsymbol{Q}$ with given $\{\boldsymbol{t}_n\}_{n=1}^N$ and $\{\boldsymbol{r}_m\}_{m=1}^M$: In this subproblem, our objective is optimizing the transmit covariance matrix $\boldsymbol{Q}$ while given the transmit MA positions $\{\boldsymbol{t}_n\}_{n=1}^N$ and receive MA positions $\{\boldsymbol{r}_m\}_{m=1}^M$. It is worth noting that, with given $\boldsymbol{H}(\tilde{\boldsymbol{t}},\tilde{\boldsymbol{r}})$, (P1) becomes a convex optimization problem for $\boldsymbol{Q}$, and the optimal solution can be obtained through eigenmode transmission [30]. Specifically, we define $\boldsymbol{H}(\tilde{\boldsymbol{t}},\tilde{\boldsymbol{r}})=\tilde{\boldsymbol{U}}\tilde{\boldsymbol{\Lambda}}\tilde{\boldsymbol{V}}^H$ as the truncated singular value decomposition (SVD) of $\boldsymbol{H}(\tilde{\boldsymbol{t}},\tilde{\boldsymbol{r}})$, where $\tilde{\boldsymbol{U}}\in\mathbb{C}^{M\times S}$, $\tilde{\boldsymbol{V}}\in\mathbb{C}^{N\times S}$, $\tilde{\boldsymbol{\Lambda}}\in\mathbb{C}^{S\times S}$, and $S=\mathrm{rank}(\boldsymbol{H}(\tilde{\boldsymbol{t}},\tilde{\boldsymbol{r}}))\leq\min(N,M)$. Therefore, the transmit precoding matrix and receive combining matrix for achieving the maximum capacity can be set as $\tilde{\boldsymbol{V}}\mathrm{diag}([\sqrt{p_1^\star},\sqrt{p_2^\star},\ldots,\sqrt{p_S^\star}])$ and $\tilde{\boldsymbol{U}}$, respectively, and the optimal solution for $\boldsymbol{Q}$ is given by

$$\boldsymbol{Q}^\star=\tilde{\boldsymbol{V}}\mathrm{diag}([p_1^\star,p_2^\star,\ldots,p_S^\star])\tilde{\boldsymbol{V}}^H, \tag{10}$$

where the power of the sth ($s=1,2,\ldots,S$) data stream, $p_s^\star$, is obtained based on the water-filling principle: $p_s^\star=\max\left(0,1/p_0-\sigma^2/\tilde{\boldsymbol{\Lambda}}[s,s]^2\right)$, with $\sum_{s=1}^S p_s^\star=P$. Thus, given $\{\boldsymbol{t}_n\}_{n=1}^N$ and $\{\boldsymbol{r}_m\}_{m=1}^M$, the MIMO channel capacity can be expressed as

$$C(\tilde{\boldsymbol{t}},\tilde{\boldsymbol{r}})=\sum_{s=1}^S\log_2\left(1+\frac{\tilde{\boldsymbol{\Lambda}}[s,s]^2p_s^\star}{\sigma^2}\right). \tag{11}$$

2) Optimization of $\boldsymbol{r}_m$ with given $\boldsymbol{Q}$, $\{\boldsymbol{r}_k,k\neq m\}_{k=1}^M$ and $\{\boldsymbol{t}_n\}_{n=1}^N$: In this subproblem, we aim to optimize $\boldsymbol{r}_m$ in (P1) with given $\boldsymbol{Q}$, $\{\boldsymbol{t}_n\}_{n=1}^N$, and $\{\boldsymbol{r}_k,k\neq m\}_{k=1}^M$, $\forall m\in\mathcal{M}=\{1,2,\ldots,M\}$. Denote the eigenvalue decomposition (EVD) of $\boldsymbol{Q}$ by $\boldsymbol{Q}=\boldsymbol{U}_Q\boldsymbol{V}_Q\boldsymbol{U}_Q^H$, with $\boldsymbol{U}_Q\in\mathbb{C}^{N\times N}$ and $\boldsymbol{V}_Q\in\mathbb{C}^{N\times N}$. It is worth noting that as the matrix $\boldsymbol{Q}$ is positive and semi-definite, all diagonal elements of $\boldsymbol{V}_Q$ are real numbers that are non-negative. Given $\{\boldsymbol{t}_n\}_{n=1}^N$ and $\boldsymbol{Q}$, we define $\boldsymbol{W}(\tilde{\boldsymbol{r}})=\boldsymbol{H}(\tilde{\boldsymbol{t}},\tilde{\boldsymbol{r}})\boldsymbol{U}_Q\boldsymbol{V}_Q^{\frac{1}{2}}\in\mathbb{C}^{M\times N}$ and denote the mth column vector of $\boldsymbol{W}(\tilde{\boldsymbol{r}})^H$ by $\boldsymbol{w}(\boldsymbol{r}_m)\in\mathbb{C}^N$, which is only determined by the position of the mth MA and can be written as

$$\boldsymbol{w}(\boldsymbol{r}_m)=\boldsymbol{V}_Q^{\frac{1}{2}}\boldsymbol{U}_Q^H\boldsymbol{G}(\tilde{\boldsymbol{t}})^H\boldsymbol{\Sigma}^H\boldsymbol{f}(\boldsymbol{r}_m). \tag{12}$$

Thus, the objective function of (P1) is written with respect to $\tilde{\boldsymbol{r}}$:

$$\begin{aligned}b(\tilde{\boldsymbol{r}})&\triangleq\log_2\det\left(\boldsymbol{I}_M+\frac{1}{\sigma^2}\boldsymbol{H}(\tilde{\boldsymbol{t}},\tilde{\boldsymbol{r}})\boldsymbol{Q}\boldsymbol{H}(\tilde{\boldsymbol{t}},\tilde{\boldsymbol{r}})^H\right)\\&=\log_2\det\left(\boldsymbol{I}_M+\frac{1}{\sigma^2}\boldsymbol{W}(\tilde{\boldsymbol{r}})\boldsymbol{W}(\tilde{\boldsymbol{r}})^H\right)\\&\overset{(a)}{=}\log_2\det\left(\boldsymbol{I}_N+\frac{1}{\sigma^2}\boldsymbol{W}(\tilde{\boldsymbol{r}})^H\boldsymbol{W}(\tilde{\boldsymbol{r}})\right)\\&=\log_2\det\left(\boldsymbol{I}_N+\frac{1}{\sigma^2}\sum_{m=1}^M\boldsymbol{w}(\boldsymbol{r}_m)\boldsymbol{w}(\boldsymbol{r}_m)^H\right),\end{aligned} \tag{13}$$

where the equality marked by (a) holds due to $\det(\boldsymbol{I}_p+\boldsymbol{A}\boldsymbol{B})=\det(\boldsymbol{I}_q+\boldsymbol{B}\boldsymbol{A})$ for $\boldsymbol{A}\in\mathbb{C}^{p\times q}$ and $\boldsymbol{B}\in\mathbb{C}^{q\times p}$. Notice from (13) that $\boldsymbol{H}(\tilde{\boldsymbol{t}},\tilde{\boldsymbol{r}})\boldsymbol{Q}\boldsymbol{H}(\tilde{\boldsymbol{t}},\tilde{\boldsymbol{r}})^H$ is in fact the summation of M rank-one matrices. To maximize the MIMO channel capacity, the M matrices should be optimally balanced by designing $\{\boldsymbol{r}_m\}_{m=1}^M$. Note that (13) explicitly decouples the

position variables for all the M MAs, i.e., $\{\boldsymbol{r}_m\}_{m=1}^M$, which facilitates the following optimization of $\boldsymbol{r}_m$.

Remove $\boldsymbol{w}(\boldsymbol{r}_m)$ from $\boldsymbol{W}(\tilde{\boldsymbol{r}})^H$ and denote the remaining $N \times (M-1)$ sub-matrix by $\boldsymbol{W}_m^H = [\boldsymbol{w}(\boldsymbol{r}_1), \boldsymbol{w}(\boldsymbol{r}_2), \ldots, \boldsymbol{w}(\boldsymbol{r}_{m-1}), \boldsymbol{w}(\boldsymbol{r}_{m+1}), \ldots, \boldsymbol{w}(\boldsymbol{r}_M)]$. Thus, the objective function of (P1) in (13) is written as [8]

$$\begin{aligned}\bar{b}(\boldsymbol{r}_m) &= \log_2 \det\left(\boldsymbol{I}_N + \frac{1}{\sigma^2}\left(\boldsymbol{W}_m^H\boldsymbol{W}_m + \boldsymbol{w}(\boldsymbol{r}_m)\boldsymbol{w}(\boldsymbol{r}_m)^H\right)\right)\\ &\overset{(b_1)}{=} \log_2 \det\Big(\boldsymbol{I}_N + \frac{1}{\sigma^2}\Big(\boldsymbol{I}_N + \frac{1}{\sigma^2}\boldsymbol{W}_m^H\boldsymbol{W}_m\Big)^{-1}\boldsymbol{w}(\boldsymbol{r}_m)\boldsymbol{w}(\boldsymbol{r}_m)^H\Big)\\ &\quad + \log_2 \det\left(\boldsymbol{I}_N + \frac{1}{\sigma^2}\boldsymbol{W}_m^H\boldsymbol{W}_m\right)\\ &\overset{(b_2)}{=} \log_2\left(1 + \frac{1}{\sigma^2}\boldsymbol{w}(\boldsymbol{r}_m)^H\Big(\boldsymbol{I}_N + \frac{1}{\sigma^2}\boldsymbol{W}_m^H\boldsymbol{W}_m\Big)^{-1}\boldsymbol{w}(\boldsymbol{r}_m)\right)\\ &\quad + \log_2 \det\left(\boldsymbol{I}_N + \frac{1}{\sigma^2}\boldsymbol{W}_m^H\boldsymbol{W}_m\right),\end{aligned} \tag{14}$$

where the equality marked by (b_1) holds due to the fact that $\det(\boldsymbol{AB}) = \det(\boldsymbol{A})\det(\boldsymbol{B})$ holds for two square matrices $\boldsymbol{A}$ and $\boldsymbol{B}$ of equal size. The equality marked by (b_2) holds because of $\det(\boldsymbol{I}_p + \boldsymbol{AB}) = \det(\boldsymbol{I}_q + \boldsymbol{BA})$ for $\boldsymbol{A} \in \mathbb{C}^{p\times q}$ and $\boldsymbol{B} \in \mathbb{C}^{q\times p}$. Notice from (14) that the maximization of $\bar{b}(\boldsymbol{r}_m)$ for given $\boldsymbol{Q}$ and $\{\boldsymbol{r}_k, k \neq m\}_{k=1}^M$ is equivalent to maximizing

$$g(\boldsymbol{r}_m) \triangleq \boldsymbol{w}(\boldsymbol{r}_m)^H \boldsymbol{A}_m \boldsymbol{w}(\boldsymbol{r}_m), \tag{15}$$

where $\boldsymbol{A}_m \triangleq \left(\boldsymbol{I}_N + \frac{1}{\sigma^2}\boldsymbol{W}_m^H\boldsymbol{W}_m\right)^{-1} \in \mathbb{C}^{N\times N}$ is a positive definite matrix independent to $\boldsymbol{r}_m$. During the iterations, to reduce the computational complexity of matrix inverse operation for $2 \leq m \leq M$, matrix $\boldsymbol{A}_m$ can be updated based on $\boldsymbol{A}_{m-1}$. Specifically, we define $\boldsymbol{Z}_1 = [\boldsymbol{w}(\boldsymbol{r}_{m-1}), \boldsymbol{w}(\boldsymbol{r}_m)] \in \mathbb{C}^{N\times 2}$ and $\boldsymbol{Z}_2 = [\boldsymbol{w}(\boldsymbol{r}_{m-1}), -\boldsymbol{w}(\boldsymbol{r}_m)] \in \mathbb{C}^{N\times 2}$ such that

$$\boldsymbol{W}_m^H\boldsymbol{W}_m = \boldsymbol{W}_{m-1}^H\boldsymbol{W}_{m-1} + \boldsymbol{Z}_1\boldsymbol{Z}_2^H. \tag{16}$$

Since $(\boldsymbol{A}+\boldsymbol{BC})^{-1} = \boldsymbol{A}^{-1} - \boldsymbol{A}^{-1}\boldsymbol{B}(\boldsymbol{I}_q + \boldsymbol{CA}^{-1}\boldsymbol{B})^{-1}\boldsymbol{CA}^{-1}$ for $\boldsymbol{A} \in \mathbb{C}^{p\times p}$, $\boldsymbol{B} \in \mathbb{C}^{p\times q}$ and $\boldsymbol{C} \in \mathbb{C}^{q\times p}$, we have [31]

$$\begin{aligned}\boldsymbol{A}_m = &\boldsymbol{A}_{m-1} - \\ &\frac{1}{\sigma^2}\boldsymbol{A}_{m-1}\boldsymbol{Z}_1\left(\boldsymbol{I}_2 + \frac{1}{\sigma^2}\boldsymbol{Z}_2^H\boldsymbol{A}_{m-1}\boldsymbol{Z}_1\right)^{-1}\boldsymbol{Z}_2^H\boldsymbol{A}_{m-1}.\end{aligned} \tag{17}$$

Furthermore, we define a positive definite matrix

$$\boldsymbol{B}_m \triangleq \boldsymbol{\Sigma}\boldsymbol{G}(\tilde{\boldsymbol{t}})\boldsymbol{U}_Q\boldsymbol{V}_Q^{\frac{1}{2}}\boldsymbol{A}_m\boldsymbol{V}_Q^{\frac{1}{2}}\boldsymbol{U}_Q^H\boldsymbol{G}(\tilde{\boldsymbol{t}})^H\boldsymbol{\Sigma}^H \in \mathbb{C}^{L_r\times L_r}. \tag{18}$$

According to (12), $g(\boldsymbol{r}_m)$ in (15) can be rewritten in the following form with respect to $\boldsymbol{f}(\boldsymbol{r}_m)$:

$$\begin{aligned}g(\boldsymbol{r}_m) &= \boldsymbol{f}(\boldsymbol{r}_m)^H\boldsymbol{\Sigma}\boldsymbol{G}(\tilde{\boldsymbol{t}})\boldsymbol{U}_Q\boldsymbol{V}_Q^{\frac{1}{2}}\boldsymbol{A}_m\boldsymbol{V}_Q^{\frac{1}{2}}\boldsymbol{U}_Q^H\boldsymbol{G}(\tilde{\boldsymbol{t}})^H\boldsymbol{\Sigma}^H\boldsymbol{f}(\boldsymbol{r}_m)\\ &= \boldsymbol{f}(\boldsymbol{r}_m)^H\boldsymbol{B}_m\boldsymbol{f}(\boldsymbol{r}_m).\end{aligned} \tag{19}$$

Notice that $\boldsymbol{B}_m$ is a constant matrix independent to $\boldsymbol{r}_m$. As a result, the subproblem for optimizing $\boldsymbol{r}_m$ can be expressed as

$$\begin{aligned}\text{(P2-m)}\quad \max_{\boldsymbol{r}_m}\quad & \boldsymbol{f}(\boldsymbol{r}_m)^H\boldsymbol{B}_m\boldsymbol{f}(\boldsymbol{r}_m) && \text{(20a)}\\ \text{s.t.}\quad & \boldsymbol{r}_m \in \mathcal{C}_r, && \text{(20b)}\\ & \|\boldsymbol{r}_m - \boldsymbol{r}_k\|_2 \geq D, \quad k = 1,2,\ldots,M, \quad k \neq m. && \text{(20c)}\end{aligned}$$

As can be observed, the objective function of (P2-m) is a non-concave function for $\boldsymbol{r}_m$. Moreover, the minimum distance constraints (20c) are also non-convex. Thus, problem (P2-m) is still a non-convex optimization problem which is difficult to solve. We will present the solution for (P2-m) in Section III-B, where the successive convex approximation (SCA) is used for relaxing this problem.

3) Optimization of $\boldsymbol{t}_n$ with given $\boldsymbol{Q}$, $\{\boldsymbol{t}_l, l \neq n\}_{l=1}^N$ and $\{\boldsymbol{r}_m\}_{m=1}^M$: In this subproblem, we aim to optimize $\boldsymbol{t}_n$ in (P1) with given $\boldsymbol{Q}$, $\{\boldsymbol{r}_m\}_{m=1}^M$, and $\{\boldsymbol{t}_l, l \neq n\}_{l=1}^N$, $\forall n \in \mathcal{N} = \{1,2,\ldots,N\}$. Since the singular values of channel matrices $\boldsymbol{H}(\tilde{\boldsymbol{t}}, \tilde{\boldsymbol{r}})$ and $\boldsymbol{H}(\tilde{\boldsymbol{t}}, \tilde{\boldsymbol{r}})^H$ are the same, the channel capacity of $\boldsymbol{H}(\tilde{\boldsymbol{t}}, \tilde{\boldsymbol{r}})$ is always equal to that of $\boldsymbol{H}(\tilde{\boldsymbol{t}}, \tilde{\boldsymbol{r}})^H$ under the same transmit power constraint, which is also known as the channel reciprocity for MIMO systems, i.e.,

$$\max_{\boldsymbol{Q}:\mathrm{Tr}(\boldsymbol{Q})\leq P, \boldsymbol{Q}\succeq\boldsymbol{0}} \log_2 \det\left(\boldsymbol{I}_M + \frac{1}{\sigma^2}\boldsymbol{H}(\tilde{\boldsymbol{t}}, \tilde{\boldsymbol{r}})\boldsymbol{Q}\boldsymbol{H}(\tilde{\boldsymbol{t}}, \tilde{\boldsymbol{r}})^H\right) \tag{21}$$

$$= \max_{\boldsymbol{S}:\mathrm{Tr}(\boldsymbol{S})\leq P, \boldsymbol{S}\succeq\boldsymbol{0}} \log_2 \det\left(\boldsymbol{I}_N + \frac{1}{\sigma^2}\boldsymbol{H}(\tilde{\boldsymbol{t}}, \tilde{\boldsymbol{r}})^H\boldsymbol{S}\boldsymbol{H}(\tilde{\boldsymbol{t}}, \tilde{\boldsymbol{r}})\right),$$

where $\boldsymbol{S} \in \mathbb{C}^{M\times M}$ is the equivalent covariance matrix of transmit signals for $\boldsymbol{H}(\tilde{\boldsymbol{t}}, \tilde{\boldsymbol{r}})^H$, with $\mathrm{Tr}(\boldsymbol{S}) \leq P$ and $\boldsymbol{S} \succeq \boldsymbol{0}$. Similar to the optimization of $\boldsymbol{Q}$ with given $\{\boldsymbol{t}_n\}_{n=1}^N$ and $\{\boldsymbol{r}_m\}_{m=1}^M$, the optimal $\boldsymbol{S}$ is given by the eigenmode transmission. Specifically, the truncated SVD of $\boldsymbol{H}(\tilde{\boldsymbol{t}}, \tilde{\boldsymbol{r}})^H$ is written as $\boldsymbol{H}(\tilde{\boldsymbol{t}}, \tilde{\boldsymbol{r}})^H = \tilde{\boldsymbol{V}}\tilde{\boldsymbol{\Lambda}}\tilde{\boldsymbol{U}}^H$. Then, the optimal $\boldsymbol{S}$ is given by

$$\boldsymbol{S}^\star = \tilde{\boldsymbol{U}}\mathrm{diag}([p_1^\star, p_2^\star, \ldots, p_S^\star])\tilde{\boldsymbol{U}}^H, \tag{22}$$

where the optimal power allocated to S date streams, $\{p_s^\star\}_{s=1}^S$, is given by (10).

Similar to the procedure for optimizing $\boldsymbol{r}_m$, we denote $\boldsymbol{S} = \boldsymbol{U}_S\boldsymbol{V}_S\boldsymbol{U}_S^H$ as the EVD of $\boldsymbol{S}$, with $\boldsymbol{U}_S \in \mathbb{C}^{M\times M}$ and $\boldsymbol{V}_S \in \mathbb{C}^{M\times M}$. As the matrix $\boldsymbol{S}$ is positive and semi-definite, all diagonal elements of $\boldsymbol{V}_S$ are real numbers that are non-negative. Then, we define $\boldsymbol{P}(\tilde{\boldsymbol{t}}) = \boldsymbol{H}(\tilde{\boldsymbol{t}}, \tilde{\boldsymbol{r}})^H\boldsymbol{U}_S\boldsymbol{V}_S^{\frac{1}{2}} \in \mathbb{C}^{N\times M}$ and denote the nth column vector of $\boldsymbol{P}(\tilde{\boldsymbol{t}})^H$ by $\boldsymbol{p}(\boldsymbol{t}_n) = \boldsymbol{V}_S^{\frac{1}{2}}\boldsymbol{U}_S^H\boldsymbol{F}(\tilde{\boldsymbol{r}})^H\boldsymbol{\Sigma}\boldsymbol{g}(\boldsymbol{t}_n) \in \mathbb{C}^M$. Then, remove $\boldsymbol{p}(\boldsymbol{t}_n)$ from $\boldsymbol{P}(\tilde{\boldsymbol{t}})^H$ and denote the remaining $M \times (N-1)$ sub-matrix by $\boldsymbol{P}_n^H = [\boldsymbol{p}(\boldsymbol{t}_1), \boldsymbol{p}(\boldsymbol{t}_2), \ldots, \boldsymbol{p}(\boldsymbol{t}_{n-1}), \boldsymbol{p}(\boldsymbol{t}_{n+1}), \ldots, \boldsymbol{p}(\boldsymbol{t}_N)]$. Let $\boldsymbol{C}_n \triangleq \left(\boldsymbol{I}_M + \frac{1}{\sigma^2}\boldsymbol{P}_n^H\boldsymbol{P}_n\right)^{-1} \in \mathbb{C}^{M\times M}$, which can be updated similarly to (17). Next, we define

$$\boldsymbol{D}_n \triangleq \boldsymbol{\Sigma}^H\boldsymbol{F}(\tilde{\boldsymbol{r}})\boldsymbol{U}_S\boldsymbol{V}_S^{\frac{1}{2}}\boldsymbol{C}_n\boldsymbol{V}_S^{\frac{1}{2}}\boldsymbol{U}_S^H\boldsymbol{F}(\tilde{\boldsymbol{r}})^H\boldsymbol{\Sigma} \in \mathbb{C}^{L_t\times L_t}. \tag{23}$$

As a result, the optimization of $\boldsymbol{t}_n$ can be expressed as

$$\begin{aligned}\text{(P3-n)}\quad \max_{\boldsymbol{t}_n}\quad & \boldsymbol{g}(\boldsymbol{t}_n)^H\boldsymbol{D}_n\boldsymbol{g}(\boldsymbol{t}_n) && \text{(24a)}\\ \text{s.t.}\quad & \boldsymbol{t}_n \in \mathcal{C}_t, && \text{(24b)}\\ & \|\boldsymbol{t}_n - \boldsymbol{t}_l\|_2 \geq D, \quad l = 1,2,\ldots,N, \quad l \neq n. && \text{(24c)}\end{aligned}$$

As can be observed, problem (P3-n) has the same structure as (P2-m). Thus, in the following, we only provide the details of the solution for problem (P2-m), and problem (P3-n) can be solved in a similar way.

B. Solution for Problem (P2-m)

To solve problem (P2-m), the SCA technique is adopted to optimize the position of the mth receive MA, $\boldsymbol{r}_m$. Although the objective function $\boldsymbol{f}(\boldsymbol{r}_m)^H\boldsymbol{B}_m\boldsymbol{f}(\boldsymbol{r}_m)$ is a non-concave function over $\boldsymbol{r}_m$, it is convex with respect to $\boldsymbol{f}(\boldsymbol{r}_m)$. Since the convex function can be globally lower-bounded by its first-order Taylor expansion at arbitrary point, we can derive the following lower bound on $\boldsymbol{f}(\boldsymbol{r}_m)^H\boldsymbol{B}_m\boldsymbol{f}(\boldsymbol{r}_m)$ with given local point $\boldsymbol{r}_m^i$ in the ith iteration of SCA [32]:

$$\begin{aligned} g(\boldsymbol{r}_m) &= \boldsymbol{f}(\boldsymbol{r}_m)^H\boldsymbol{B}_m\boldsymbol{f}(\boldsymbol{r}_m) \\ &\geq \boldsymbol{f}(\boldsymbol{r}_m^i)^H\boldsymbol{B}_m\boldsymbol{f}(\boldsymbol{r}_m^i) \\ &\quad + 2\mathrm{Re}\left\{\boldsymbol{f}(\boldsymbol{r}_m^i)^H\boldsymbol{B}_m\left(\boldsymbol{f}(\boldsymbol{r}_m)-\boldsymbol{f}(\boldsymbol{r}_m^i)\right)\right\} \\ &= \underbrace{2\,\mathrm{Re}\left\{\boldsymbol{f}(\boldsymbol{r}_m^i)^H\boldsymbol{B}_m\boldsymbol{f}(\boldsymbol{r}_m)\right\}}_{\bar{g}(\boldsymbol{r}_m)} - \underbrace{\boldsymbol{f}(\boldsymbol{r}_m^i)^H\boldsymbol{B}_m\boldsymbol{f}(\boldsymbol{r}_m^i)}_{\text{constant}}, \end{aligned} \tag{25}$$

where $\boldsymbol{r}_m^i \in \mathbb{R}^2$ is a constant vector which represents the value of $\boldsymbol{r}_m$ in the ith iteration. Thus, maximizing $\boldsymbol{f}(\boldsymbol{r}_m)^H\boldsymbol{B}_m\boldsymbol{f}(\boldsymbol{r}_m)$ can be simplified to maximizing $\bar{g}(\boldsymbol{r}_m) \triangleq \mathrm{Re}\left\{\boldsymbol{f}(\boldsymbol{r}_m^i)^H\boldsymbol{B}_m\boldsymbol{f}(\boldsymbol{r}_m)\right\}$. Although $\bar{g}(\boldsymbol{r}_m)$ is a linear function over $\boldsymbol{f}(\boldsymbol{r}_m)$, it is still neither concave nor convex over $\boldsymbol{r}_m$. Thus, we cannot construct the surrogate function lower-bounding the objective function only by the first-order Taylor expansion of $\bar{g}(\boldsymbol{r}_m)$. Alternatively, we construct a surrogate function that locally approximates the objective function by using the second-order Taylor expansion. Denote the gradient vector and Hessian matrix of $\bar{g}(\boldsymbol{r}_m)$ over $\boldsymbol{r}_m$ by $\nabla\bar{g}(\boldsymbol{r}_m) \in \mathbb{R}^2$ and $\nabla^2\bar{g}(\boldsymbol{r}_m) \in \mathbb{R}^{2\times 2}$, respectively, with their derivations provided in Appendix A. Then, we construct a positive real number δ_m making $\delta_m\boldsymbol{I}_2 \succeq \nabla^2\bar{g}(\boldsymbol{r}_m)$, with the closed-form expression given in Appendix B. Thus, based on Taylor's theorem, we can find a quadratic surrogate function to globally lower-bound the objective function $\bar{g}(\boldsymbol{r}_m)$ as [33]

$$\begin{aligned} \bar{g}(\boldsymbol{r}_m) &\geq \bar{g}(\boldsymbol{r}_m^i) + \nabla\bar{g}(\boldsymbol{r}_m^i)^T\left(\boldsymbol{r}_m-\boldsymbol{r}_m^i\right) \\ &\quad - \frac{\delta_m}{2}\left(\boldsymbol{r}_m-\boldsymbol{r}_m^i\right)^T\left(\boldsymbol{r}_m-\boldsymbol{r}_m^i\right) \\ &= \underbrace{-\frac{\delta_m}{2}\boldsymbol{r}_m^T\boldsymbol{r}_m + \left(\nabla\bar{g}(\boldsymbol{r}_m^i)+\delta_m\boldsymbol{r}_m^i\right)^T\boldsymbol{r}_m}_{\tilde{g}(\boldsymbol{r}_m)} \\ &\quad + \underbrace{\bar{g}(\boldsymbol{r}_m^i) - \frac{\delta_m}{2}(\boldsymbol{r}_m^i)^T\boldsymbol{r}_m^i}_{\text{constant}}. \end{aligned} \tag{26}$$

Thus, maximizing $\bar{g}(\boldsymbol{r}_m)$ can be converted to maximizing $\tilde{g}(\boldsymbol{r}_m) \triangleq -\frac{\delta_m}{2}\boldsymbol{r}_m^T\boldsymbol{r}_m + (\nabla\bar{g}(\boldsymbol{r}_m^i)+\delta_m\boldsymbol{r}_m^i)^T\boldsymbol{r}_m$. To this end, in the ith iteration of SCA, the optimization problem of the mth receive MA position $\boldsymbol{r}_m$ can be relaxed as

$$\text{(P4-m)} \quad \max_{\boldsymbol{r}_m} \quad -\frac{\delta_m}{2}\boldsymbol{r}_m^T\boldsymbol{r}_m + \left(\nabla\bar{g}(\boldsymbol{r}_m^i)+\delta_m\boldsymbol{r}_m^i\right)^T\boldsymbol{r}_m \tag{27}$$

$$\text{s.t.} \quad \text{(20b)}, \text{(20c)}.$$

Since the objective function of (P4-m) is a concave quadratic function over $\boldsymbol{r}_m$, the global optimum for maximizing $\tilde{g}(\boldsymbol{r}_m)$ by neglecting constraints (20b) and (20c) is obtained in closed form as

$$\boldsymbol{r}_{m,i+1}^\star = \frac{1}{\delta_m}\nabla\bar{g}(\boldsymbol{r}_m^i) + \boldsymbol{r}_m^i. \tag{28}$$

If $\boldsymbol{r}_{m,i+1}^\star$ satisfies (20b) and (20c), it is the global optimum for problem (P4-m). However, if $\boldsymbol{r}_{m,i+1}^\star$ does not satisfy (20b) or (20c), we cannot obtain the optimal solution due to the non-convex constraints (20c) [4]. In this case, we propose the following solution. Denote the gradient vector of $\|\boldsymbol{r}_m-\boldsymbol{r}_k\|_2$ over $\boldsymbol{r}_m$ as $\nabla\|\boldsymbol{r}_m-\boldsymbol{r}_k\|_2 = (\boldsymbol{r}_m-\boldsymbol{r}_k)/\|\boldsymbol{r}_m-\boldsymbol{r}_k\|_2$. Since the denominator term $\|\boldsymbol{r}_m-\boldsymbol{r}_k\|_2 \geq D > 0$, the gradient vector always exists. As $\|\boldsymbol{r}_m-\boldsymbol{r}_k\|_2$ is a convex function over $\boldsymbol{r}_m$, the following inequality holds utilizing the first-order Taylor expansion at $\boldsymbol{r}_m^i$:

$$\begin{aligned} &\|\boldsymbol{r}_m-\boldsymbol{r}_k\|_2 \geq \|\boldsymbol{r}_m^i-\boldsymbol{r}_k\|_2 + \left(\nabla\|\boldsymbol{r}_m^i-\boldsymbol{r}_k\|_2\right)^T(\boldsymbol{r}_m-\boldsymbol{r}_m^i) \\ &= \|\boldsymbol{r}_m^i-\boldsymbol{r}_k\|_2 + \frac{1}{\|\boldsymbol{r}_m^i-\boldsymbol{r}_k\|_2}(\boldsymbol{r}_m^i-\boldsymbol{r}_k)^T(\boldsymbol{r}_m-\boldsymbol{r}_m^i) \\ &= \frac{1}{\|\boldsymbol{r}_m^i-\boldsymbol{r}_k\|_2}(\boldsymbol{r}_m^i-\boldsymbol{r}_k)^T(\boldsymbol{r}_m-\boldsymbol{r}_k). \end{aligned} \tag{29}$$

Hereto, for a given $\boldsymbol{r}_m^i$ obtained in the ith iteration, if $\boldsymbol{r}_{m,i+1}^\star$ does not satisfy (20b) or (20c), the convex position optimization problem for the mth receive MA is transformed into

$$\text{(P5-m)} \quad \max_{\boldsymbol{r}_m} \quad -\frac{\delta_m}{2}\boldsymbol{r}_m^T\boldsymbol{r}_m + \left(\nabla\bar{g}(\boldsymbol{r}_m^i)+\delta_m\boldsymbol{r}_m^i\right)^T\boldsymbol{r}_m \tag{30a}$$

$$\text{s.t.} \quad \frac{1}{\|\boldsymbol{r}_m^i-\boldsymbol{r}_k\|_2}(\boldsymbol{r}_m^i-\boldsymbol{r}_k)^T(\boldsymbol{r}_m-\boldsymbol{r}_k) \geq D, \quad k=1,2,\ldots,M, \quad k\neq m, \tag{30b}$$

$$\text{(20b)}.$$

Since the objective function (30a) is quadratic and constraints (30b) are linear with respect to $\boldsymbol{r}_m$, (P5-m) is a quadratic programming (QP) problem and can be efficiently solved by using quadprog [34]. The details of the proposed algorithm to solve problem (P2-m) are summarized in Algorithm 1. Specifically, from step 4 to step 6, we compute the gradient vector and Hessian matrix of $\bar{g}(\boldsymbol{r}_m)$ at $\boldsymbol{r}_m^i$ via (40) and (41), respectively, and then obtain δ_m via (43). Then, we obtain $\boldsymbol{r}_{m,i+1}^\star$ as the global optimum to maximize $\tilde{g}(\boldsymbol{r}_m)$ in step 7. If $\boldsymbol{r}_{m,i+1}^\star$ satisfies (20b) and (20c), we set it as $\boldsymbol{r}_m^{i+1}$ for the next iteration. Otherwise we solve the QP problem (30) to obtain $\boldsymbol{r}_m^{i+1}$ in step 11. The proposed algorithm terminates when the increase of the objective value in (20a) is below ϵ_1, which is a predefined convergence threshold. Finally, we output the position of the mth receive MA in step 15.

Next we analyze the convergence of the proposed Algorithm 1. Denote the two constant terms in (25) and (26) by $\Gamma_1(\boldsymbol{r}_m^i) = -\boldsymbol{f}(\boldsymbol{r}_m^i)^H\boldsymbol{B}_m\boldsymbol{f}(\boldsymbol{r}_m^i)$ and $\Gamma_2(\boldsymbol{r}_m^i) = \bar{g}(\boldsymbol{r}_m^i) - \frac{\delta_m}{2}(\boldsymbol{r}_m^i)^T\boldsymbol{r}_m^i$, respectively. Then, for the ith iteration, the

[4]To reduce the computational complexity of the proposed algorithm and time overhead of antenna movement in practical scenarios, the transmit/receive region can be divided into N/M sub-regions, where each MA can move freely in its corresponding sub-region enabled by an independent driver. In this case, we can obtain the optimal solution for problem (P4-m) for some typical convex sub-regions in closed form, as shown in (35) and (36).

Algorithm 1 SCA for Solving Problem (P2-m)

Input: M, L_r, $\{\boldsymbol{r}_k, k \neq m\}_{k=1}^{M}$, $\boldsymbol{B}_m$, $\{\theta_r^q\}_{q=1}^{L_r}$, $\{\phi_r^q\}_{q=1}^{L_r}$, $\mathcal{C}_r$, D, ϵ_1, $\boldsymbol{r}_m^0$.
Initialization: $i \leftarrow 0$.
while Increase of the objective value in (20a) is above ϵ_1 **do**
  Obtain $\boldsymbol{b}$ via (38).
  Compute $\nabla \bar{g}(\boldsymbol{r}_m^i)$ and $\nabla^2 \bar{g}(\boldsymbol{r}_m^i)$ via (40) and (41), respectively.
  Update δ_m via (43).
  Obtain $\boldsymbol{r}_{m,i+1}^{\star}$ via (28).
  if $\boldsymbol{r}_{m,i+1}^{\star}$ satisfies (20b) and (20c) **then**
    $\boldsymbol{r}_m^{i+1} \leftarrow \boldsymbol{r}_{m,i+1}^{\star}$.
  else
    Obtain $\boldsymbol{r}_m^{i+1}$ by solving (30).
  end if
  $i \leftarrow i + 1$.
end while
Output: $\boldsymbol{r}_m$.

objective function in (20a) can be written as

$$\begin{aligned} g(\boldsymbol{r}_m^i) &\overset{(c_1)}{=} 2\left(\tilde{g}(\boldsymbol{r}_m^i) + \Gamma_2(\boldsymbol{r}_m^i)\right) + \Gamma_1(\boldsymbol{r}_m^i) \\ &\overset{(c_2)}{\leq} 2\left(\tilde{g}(\boldsymbol{r}_m^{i+1}) + \Gamma_2(\boldsymbol{r}_m^i)\right) + \Gamma_1(\boldsymbol{r}_m^i) \\ &\overset{(c_3)}{\leq} 2\bar{g}(\boldsymbol{r}_m^{i+1}) + \Gamma_1(\boldsymbol{r}_m^i) \overset{(c_4)}{\leq} g(\boldsymbol{r}_m^{i+1}), \end{aligned} \tag{31}$$

where the equality marked by (c_1) holds because the first-order Taylor expansion in (25) and the second-order Taylor expansion in (26) are tight at $\boldsymbol{r}_m^i$. The inequality marked by (c_2) holds because we maximize the value of $\tilde{g}(\boldsymbol{r}_m)$ in the ith iteration, and the equality can be achieved by choosing $\boldsymbol{r}_m^{i+1} = \boldsymbol{r}_m^i$. The inequalities marked by (c_3) and (c_4) hold because $\tilde{g}(\boldsymbol{r}_m) + \Gamma_2(\boldsymbol{r}_m^i)$ and $2\bar{g}(\boldsymbol{r}_m) + \Gamma_1(\boldsymbol{r}_m^i)$ are lower bounds on $\bar{g}(\boldsymbol{r}_m)$ and $g(\boldsymbol{r}_m)$ at $\boldsymbol{r}_m^{i+1}$, respectively. Thus, sequence $\{g(\boldsymbol{r}_m^i)\}_{i=0}^{\infty}$ is non-decreasing and will converge to a maximum value.

In the following, we analyze the computational complexity of Algorithm 1. Specifically, from step 4 to step 7, the complexities of calculating $\boldsymbol{b}$, $\nabla \bar{g}(\boldsymbol{r}_m^i)$, $\nabla^2 \bar{g}(\boldsymbol{r}_m^i)$, δ_m, and $\boldsymbol{r}_{m,i+1}^{\star}$ are $\mathcal{O}(NL_r)$, $\mathcal{O}(L_r)$, $\mathcal{O}(L_r)$, $\mathcal{O}(1)$, and $\mathcal{O}(1)$, respectively. In step 11, the complexity to solve the QP problem (P5-m) is $\mathcal{O}(M^{1.5}\ln(1/\beta))$ with accuracy β for the interior-point method [35]. Let γ_r^1 and γ_r^2 denote the maximum number of inner iterations (i.e., iterations to repeat steps 4-13) and the maximum number of iterations required to perform step 11, respectively. Thus, the total complexity of Algorithm 1 is $\mathcal{O}(NL_r\gamma_r^1 + M^{1.5}\ln(1/\beta)\gamma_r^2)$, which is polynomial over N, L_r, and M.

C. Solution for Problem (P3-n)

Since problem (P3-n) has a similar structure as (P2-m), we can modify Algorithm 1 to obtain the position of the nth transmit MA $\boldsymbol{t}_n$ by replacing

$$\left\{M, L_r, \boldsymbol{r}_m, \boldsymbol{B}_m, \mathcal{C}_r, \{\boldsymbol{r}_k, k \neq m\}_{k=1}^{M}, \{\theta_r^q\}_{q=1}^{L_r}, \{\phi_r^q\}_{q=1}^{L_r}\right\}$$

Algorithm 2 Alternating Optimization for Solving Problem (P1)

Input: $\boldsymbol{\Sigma}$, P, σ, M, N, L_r, L_t, $\{\theta_r^q\}_{q=1}^{L_r}$, $\{\phi_r^q\}_{q=1}^{L_r}$, $\{\theta_t^p\}_{p=1}^{L_t}$, $\{\phi_t^p\}_{p=1}^{L_t}$, $\mathcal{C}_r$, $\mathcal{C}_t$, D, ϵ_1, ϵ_2.
Initialize $\{\boldsymbol{r}_m\}_{m=1}^{M}$ and $\{\boldsymbol{t}_n\}_{n=1}^{N}$.
while Increase of the channel capacity in (8) is above ϵ_2 **do**
  Given $\{\boldsymbol{r}_m\}_{m=1}^{M}$ and $\{\boldsymbol{t}_n\}_{n=1}^{N}$, obtain the optimal $\boldsymbol{Q}$ of (P1) via (10).
  for $m = 1 \rightarrow M$ **do**
    Obtain $\boldsymbol{B}_m$ via (18).
    Given $\boldsymbol{Q}$, $\{\boldsymbol{r}_k, k \neq m\}_{k=1}^{M}$, and $\{\boldsymbol{t}_n\}_{n=1}^{N}$, solve problem (P2-m) to update $\boldsymbol{r}_m$.
  end for
  Calculate $\boldsymbol{S}^{\star}$ via (22).
  for $n = 1 \rightarrow N$ **do**
    Obtain $\boldsymbol{D}_n$ via (23).
    Given $\boldsymbol{Q}$, $\{\boldsymbol{t}_l, l \neq n\}_{l=1}^{N}$, and $\{\boldsymbol{r}_m\}_{m=1}^{M}$, solve problem (P3-n) to update $\boldsymbol{t}_n$.
  end for
end while
Output: $\tilde{\boldsymbol{t}}$, $\tilde{\boldsymbol{r}}$, $\boldsymbol{Q}$.

with

$$\left\{N, L_t, \boldsymbol{t}_n, \boldsymbol{D}_n, \mathcal{C}_t, \{\boldsymbol{t}_l, l \neq n\}_{l=1}^{N}, \{\theta_t^p\}_{p=1}^{L_t}, \{\phi_t^p\}_{p=1}^{L_t}\right\}.$$

Similarly, the monotonic convergence is guaranteed for solving problem (P3-n) with Algorithm 1. The corresponding computational complexity is $\mathcal{O}(ML_t\gamma_t^1 + N^{1.5}\ln(1/\beta)\gamma_t^2)$, with γ_t^1 and γ_t^2 denoting the maximum number of iterations to perform steps 4-13 and step 11, respectively.

D. Overall Algorithm

With the solutions for problem (P2-m) and (P3-n) obtained above, we now finalize the proposed alternating optimization algorithm to solve (P1). The overall algorithm is summarized in Algorithm 2. Specifically, in step 4, we first obtain the optimal $\boldsymbol{Q}$ of (P1) with fixed $\{\boldsymbol{r}_m\}_{m=1}^{M}$ and $\{\boldsymbol{t}_n\}_{n=1}^{N}$ shown in (10). Then, from step 5 to step 8, we optimize the positions of M receive MAs sequentially by solving problem (P2-m) based on SCA. Similarly, from step 10 to step 13, the positions of N transmit MAs are optimized by solving problem (P3-n) successively. The algorithm solves the three subproblems iteratively, until the increase of the channel capacity in (8) is below ϵ_2, which is a predefined convergence threshold.

The convergence of the proposed Algorithm 2 is analyzed as follows. The alternating optimization of variables $\{\boldsymbol{t}_n\}_{n=1}^{N}$, $\{\boldsymbol{r}_m\}_{m=1}^{M}$, and $\boldsymbol{Q}$ guarantees that the algorithm produces a non-decreasing sequence of objective values for (P1) during the iterations, which will not go to infinity due to the finite channel capacity. Since the convergence criterion of Algorithm 2 is the inability to further increase the objective value of (P1) by optimizing any variable in $\{\boldsymbol{t}_n\}_{n=1}^{N}$, $\{\boldsymbol{r}_m\}_{m=1}^{M}$, and $\boldsymbol{Q}$, Algorithm 2 is guaranteed to converge to a solution of (P1) that is (at least) locally optimal.

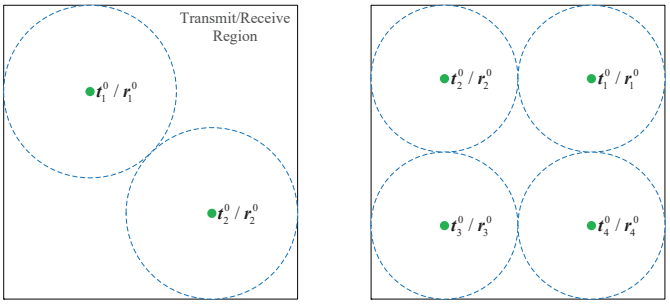

Fig. 3. An example of transmit/receive MA positioning initialization based on circle packing for $N(M) = 2$ (left) and $N(M) = 4$ (right).

The computational complexity of Algorithm 2 is analyzed as follows. Specifically, in step 4 and step 9, the complexity to calculate $\boldsymbol{Q}^\star$ and $\boldsymbol{S}^\star$ based on water-filling is $\mathcal{O}(MN\min(M,N))$ [36]. Thus, the total complexity is $\mathcal{O}((MNL_r\gamma_r^1 + M^{2.5}\ln(1/\beta)\gamma_r^2 + MNL_t\gamma_t^1 + N^{2.5}\ln(1/\beta)\gamma_t^2 + MN\min(M,N))\gamma)$ with γ denoting the maximum number of outer iterations for repeating steps 4–13 in Algorithm 2.

E. Initialization

In the following subsection, we propose an initialization scheme with low-complexity for the transmit/receive MA positions design in Algorithm 2 based on the circle packing scheme [37]. Intuitively, all the transmit/receive MAs should be sufficiently separated for the following two reasons. On one hand, increasing the distance between MAs can reduce their coupling effect. One the other hand, during the SCA process, it is more likely for each MA to update the position with the largest capacity in its neighborhood satisfying the minimum distance constraints. Under such case, we can easily set $\boldsymbol{r}_{m,i+1}^\star$ in (28) as the optimal solution for problem (P4-m) instead of relaxing it into (P5-m). Therefore, we propose that the initial positions of the MAs are obtained based on circle packing. As shown in Fig. 3, we assume that each MA occupies an initial circle region with equal radius. Then, we arrange N (or M) circles with the maximum radius in $\mathcal{C}_t$ (or $\mathcal{C}_r$) such that no overlapping among them occurs. The centers of the arranged N (or M) circles are set as the initial MA positions $\{\boldsymbol{t}_n^0\}_{n=1}^N$ (or $\{\boldsymbol{r}_m^0\}_{m=1}^M$).

F. Alternative Solution for Problem (P1) in the Low-SNR Regime

In the preceding subsections, an alternating optimization algorithm has been proposed to deal with the capacity maximization problem for the general MIMO channel. In this subsection, we investigate the particular case in the low-SNR regime, and represent the channel capacity in the more manageable form with respect to the positions of transmit and receive MAs, based on which we propose an alternative algorithm for solving the capacity maximization problem with lower complexity.

The low-SNR regime may occur in practice due to the low transmission power or large propagation distance between the transmitter and the receiver. In such case, the optimal transmission scheme is the strongest eigenmode beamforming that concentrates the transmit power to the strongest eigenchannel [30]. Specifically, denoting $\boldsymbol{Q} = P\boldsymbol{u}_Q\boldsymbol{u}_Q^H$ with $\boldsymbol{u}_Q \in \mathbb{C}^N$ being the transmit beamforming vector, then the capacity in the low-SNR regime can be represented as

$$\begin{aligned} C_L(\tilde{\boldsymbol{t}},\tilde{\boldsymbol{r}}) &= \max_{\boldsymbol{u}_Q:\|\boldsymbol{u}_Q\|_2^2=1} \log_2\det\Big(\boldsymbol{I}_M + \frac{P}{\sigma^2}\boldsymbol{H}(\tilde{\boldsymbol{t}},\tilde{\boldsymbol{r}})\boldsymbol{u}_Q \\ &\quad \times \boldsymbol{u}_Q^H\boldsymbol{H}(\tilde{\boldsymbol{t}},\tilde{\boldsymbol{r}})^H\Big) \\ &\overset{(d)}{=} \max_{\boldsymbol{u}_Q:\|\boldsymbol{u}_Q\|_2^2=1} \log_2\left(1 + \frac{P}{\sigma^2}\|\boldsymbol{H}(\tilde{\boldsymbol{t}},\tilde{\boldsymbol{r}})\boldsymbol{u}_Q\|_2^2\right), \end{aligned} \tag{32}$$

where the equality marked by (d) can be derived because of $\det(\boldsymbol{I}_p + \boldsymbol{A}\boldsymbol{B}) = \det(\boldsymbol{I}_q + \boldsymbol{B}\boldsymbol{A})$ for $\boldsymbol{A} \in \mathbb{C}^{p\times q}$ and $\boldsymbol{B} \in \mathbb{C}^{q\times p}$. As shown in (32), maximizing channel capacity in the low-SNR regime is equivalent to maximizing $\|\boldsymbol{H}(\tilde{\boldsymbol{t}},\tilde{\boldsymbol{r}})\boldsymbol{u}_Q\|_2^2$. Given $\boldsymbol{H}(\tilde{\boldsymbol{t}},\tilde{\boldsymbol{r}})$, the optimal $\boldsymbol{u}_Q$ is the strongest right singular vector of $\boldsymbol{H}(\tilde{\boldsymbol{t}},\tilde{\boldsymbol{r}})$. Besides, we denote $\boldsymbol{c} = \boldsymbol{\Sigma}\boldsymbol{G}(\tilde{\boldsymbol{t}})\boldsymbol{u}_Q \in \mathbb{C}^{L_r}$. Then, we have $\|\boldsymbol{H}(\tilde{\boldsymbol{t}},\tilde{\boldsymbol{r}})\boldsymbol{u}_Q\|_2^2 = \sum_{m=1}^M |\boldsymbol{c}^H\boldsymbol{f}(\boldsymbol{r}_m)|^2$. Given $\boldsymbol{u}_Q$, $\{\boldsymbol{r}_k, k\neq m\}_{k=1}^M$, and $\{\boldsymbol{t}_n\}_{n=1}^N$, maximizing the channel capacity in (32) is equivalent to maximizing $|\boldsymbol{c}^H\boldsymbol{f}(\boldsymbol{r}_m)|^2$ with respect to each $\boldsymbol{r}_m$. Thus, the subproblem for optimizing $\boldsymbol{r}_m$ can be formulated similarly to problem (P2-m) by replacing $\boldsymbol{B}_m$ with $\boldsymbol{c}\boldsymbol{c}^H$, which has a lower computational complexity during the iterations. Moreover, given $\boldsymbol{u}_Q$, $\{\boldsymbol{t}_l, l\neq n\}_{l=1}^N$, and $\{\boldsymbol{r}_m\}_{m=1}^M$, the optimal $\boldsymbol{S}$ is given by $\boldsymbol{S} = P\boldsymbol{u}_S\boldsymbol{u}_S^H$ with $\boldsymbol{u}_S \in \mathbb{C}^M$ being the strongest right singular vector of $\boldsymbol{H}(\tilde{\boldsymbol{t}},\tilde{\boldsymbol{r}})^H$. Defining $\boldsymbol{d} \triangleq \boldsymbol{\Sigma}^H\boldsymbol{F}(\tilde{\boldsymbol{r}})\boldsymbol{u}_S \in \mathbb{C}^{L_t}$, the subproblem for optimizing $\boldsymbol{t}_n$ can be expressed similarly to problem (P3-n) by replacing $\boldsymbol{D}_n$ with $\boldsymbol{d}\boldsymbol{d}^H$.

As a result, by iteratively optimizing one single variable in $\{\boldsymbol{t}_n\}_{n=1}^N$, $\{\boldsymbol{r}_m\}_{m=1}^M$, and $\boldsymbol{u}_Q$ with the other $M+N$ variables being fixed, an alternating optimization algorithm similar as Algorithm 2 can be employed to obtain a locally optimal solution for maximizing channel capacity in the low-SNR regime. The required complexity of the overall algorithm is given by $\mathcal{O}((L_r\gamma_r^1 + M^{2.5}\ln(1/\beta)\gamma_r^2 + L_t\gamma_t^1 + N^{2.5}\ln(1/\beta)\gamma_t^2 + MN\min(M,N))\gamma)$, which is lower than the general case of Algorithm 2 because $\boldsymbol{c}$ and $\boldsymbol{d}$ are fixed in the inner SCA iterations for solving problems (P2-m) and (P3-n).

G. Alternative Solution for Problem (P1) with Single-Antenna Transmitter/Receiver

In the previous subsection, by considering $N \geq 1$ and $M \geq 1$, we have studied (P1) for the general MIMO channel to transmit multiple data streams in parallel. In the following subsection, we investigate (P1) for the particular cases where $N = 1$ or $M = 1$, which restrict the transmission of one data stream. As a result, the expressions for the optimal transmit covariance matrix and the channel capacity can be simplified, allowing for simpler alternating optimization algorithms to solve (P1) with significantly lower complexity compared to Algorithm 2.

First, (P1) is investigated for the MISO case with $N > 1$ and $M = 1$. The field response matrix of the receive region, $\boldsymbol{F}(\tilde{\boldsymbol{r}})$, can be rewritten as vector $\boldsymbol{f}(\boldsymbol{r}) \in \mathbb{C}^{L_r}$, where $\boldsymbol{r}$ represents

the position of the receive MA. The effective channel row vector can be written as $\boldsymbol{h}(\tilde{\boldsymbol{t}},\boldsymbol{r})^H = \boldsymbol{f}(\boldsymbol{r})^H\boldsymbol{\Sigma}\boldsymbol{G}(\tilde{\boldsymbol{t}}) \in \mathbb{C}^{1\times N}$. The optimal transmit covariance matrix in the MISO case is obtained according to the maximum ratio transmission (MRT), i.e., $\boldsymbol{Q}^\star = P\boldsymbol{h}(\tilde{\boldsymbol{t}},\boldsymbol{r})\boldsymbol{h}(\tilde{\boldsymbol{t}},\boldsymbol{r})^H/\|\boldsymbol{h}(\tilde{\boldsymbol{t}},\boldsymbol{r})\|_2^2$. Thus, the MISO channel capacity is expressed as

$$\begin{aligned} C_{\text{MISO}}(\tilde{\boldsymbol{t}},\boldsymbol{r}) &= \log_2\left(1+\frac{1}{\sigma^2}\boldsymbol{h}(\tilde{\boldsymbol{t}},\boldsymbol{r})^H\boldsymbol{Q}^\star\boldsymbol{h}(\tilde{\boldsymbol{t}},\boldsymbol{r})\right) \\ &= \log_2\left(1+\frac{P}{\sigma^2}\|\boldsymbol{h}(\tilde{\boldsymbol{t}},\boldsymbol{r})\|_2^2\right). \end{aligned} \tag{33}$$

In this case, problem (P1) is converted to the equivalent problem to maximize total channel power, $\|\boldsymbol{h}(\tilde{\boldsymbol{t}},\boldsymbol{r})\|_2^2$, via optimizing $\tilde{\boldsymbol{t}}$ and $\boldsymbol{r}$

$$\begin{aligned} \text{(P1-MISO)}\quad \max_{\tilde{\boldsymbol{t}},\boldsymbol{r}}\quad & \|\boldsymbol{h}(\tilde{\boldsymbol{t}},\boldsymbol{r})\|_2^2 \\ \text{s.t.}\quad & \text{(9b), (9c), (9d).} \end{aligned} \tag{34}$$

Given $\{\boldsymbol{t}_n\}_{n=1}^N$, the subproblem for optimizing $\boldsymbol{r}$ can be formulated similarly to problem (P2-m) by setting $\boldsymbol{B}_m \leftarrow \boldsymbol{\Sigma}\boldsymbol{G}(\tilde{\boldsymbol{t}})\boldsymbol{G}(\tilde{\boldsymbol{t}})^H\boldsymbol{\Sigma}^H \in \mathbb{C}^{L_r\times L_r}$. Note that the non-convex minimum distance constraints (9e) are removed since there is only a single MA in the receive region. Then, by dropping the corresponding non-convex constraints (20c), problem (P4-m) is a convex QP problem, which can be solved efficiently without relaxation into problem (P5-m). Moreover, we can obtain the optimal solution for problem (P4-m) for some typical convex $\mathcal{C}_r$ based on $\boldsymbol{r}_{m,i+1}^\star = [x_{i+1}^\star, y_{i+1}^\star]^T$ in (28). For example, if $\mathcal{C}_r$ is a rectangle region $\{[x,y]^T | x_L \le x \le x_H, y_L \le y \le y_H\}$, then the optimal solution for problem (P4-m) is given by [38]

$$\boldsymbol{r}_m^{i+1} = [\mathcal{P}_{\text{rec}}(x_{i+1}^\star, x_L, x_H), \mathcal{P}_{\text{rec}}(y_{i+1}^\star, y_L, y_H)]^T, \tag{35}$$

where $\mathcal{P}_{\text{rec}}(x, x_L, x_H) = \min(\max(x, x_L), x_H)$ is the projection function associated with the rectangle region. Similarly, if $\mathcal{C}_r$ is a circle region $\{\boldsymbol{r} | \|\boldsymbol{r}-\boldsymbol{r}_0\|_2 \le D_0\}$ centered at point $\boldsymbol{r}_0$ with radius of D_0, the optimal solution for problem (P4-m) can be written as

$$\boldsymbol{r}_m^{i+1} = \mathcal{P}_{\text{cir}}(\boldsymbol{r}_{m,i+1}^\star - \boldsymbol{r}_0, D_0) + \boldsymbol{r}_0, \tag{36}$$

with the projector $\mathcal{P}_{\text{cir}}(\boldsymbol{r}, D) = \min(D/\|\boldsymbol{r}\|_2, 1)\boldsymbol{r}$.

Moreover, we denote $\bar{\boldsymbol{d}} = \boldsymbol{\Sigma}^H\boldsymbol{f}(\boldsymbol{r}) \in \mathbb{C}^{L_t}$. Then, we have $\|\boldsymbol{h}(\tilde{\boldsymbol{t}},\boldsymbol{r})\|_2^2 = \|\bar{\boldsymbol{d}}^H\boldsymbol{G}(\tilde{\boldsymbol{t}})\|_2^2 = \sum_{n=1}^N |\bar{\boldsymbol{d}}^H\boldsymbol{g}(\boldsymbol{t}_n)|^2$. Given $\boldsymbol{r}$ and $\{\boldsymbol{t}_l, l\neq n\}_{l=1}^N$, maximizing the channel total power in problem (P1-MISO) is equivalent to maximizing $|\bar{\boldsymbol{d}}^H\boldsymbol{g}(\boldsymbol{t}_n)|^2$ with respect to each $\boldsymbol{t}_n$. Thus, the subproblem for optimizing $\boldsymbol{t}_n$ can be formulated similarly to problem (P3-n) by replacing $\boldsymbol{D}_n$ with $\bar{\boldsymbol{d}}\bar{\boldsymbol{d}}^H$.

Therefore, we can obtain a locally optimal solution to (P1-MISO) by iteratively optimizing one variable in $\boldsymbol{r}\cup\{\boldsymbol{t}_n\}_{n=1}^N$ with the other N variables being fixed at each time. This algorithm requires a complexity of $\mathcal{O}((NL_r + L_r\gamma_r^1 + L_t\gamma_t^1 + N^{2.5}\ln(1/\beta)\gamma_t^2)\gamma)$. It is noteworthy that the complexity of the alternative algorithm is lower compared to Algorithm 2 with $M=1$. This is due to the explicit expression of the MISO channel capacity as a function of $\tilde{\boldsymbol{t}}$ and $\boldsymbol{r}$ exclusively, thus eliminating the need of iteratively solving $\boldsymbol{Q}$ in the alternating optimization.

Next, we consider the SIMO system with $M>1$ and $N=1$, where the field response matrix of the transmit region $\boldsymbol{G}(\tilde{\boldsymbol{t}})$ can be rewritten as the vector $\boldsymbol{g}(\boldsymbol{t}) \in \mathbb{C}^{L_t}$ with $\boldsymbol{t}$ representing the position of the transmit MA. The SIMO channel is thus given by $\boldsymbol{h}(\boldsymbol{t},\tilde{\boldsymbol{r}}) = \boldsymbol{F}(\tilde{\boldsymbol{r}})^H\boldsymbol{\Sigma}\boldsymbol{g}(\boldsymbol{t}) \in \mathbb{C}^M$. It should be noted that for the case of $N=1$, the optimal transmit covariance matrix is readily set as $\boldsymbol{Q}^\star = P$, leading to the corresponding channel capacity:

$$\begin{aligned} C_{\text{SIMO}}(\boldsymbol{t},\tilde{\boldsymbol{r}}) &= \log_2\det\left(\boldsymbol{I}_M + \frac{1}{\sigma^2}\boldsymbol{h}(\boldsymbol{t},\tilde{\boldsymbol{r}})\boldsymbol{Q}\boldsymbol{h}(\boldsymbol{t},\tilde{\boldsymbol{r}})^H\right) \\ &\overset{(e)}{=} \log_2\left(1+\frac{P}{\sigma^2}\|\boldsymbol{h}(\boldsymbol{t},\tilde{\boldsymbol{r}})\|_2^2\right), \end{aligned} \tag{37}$$

where the equality marked by (e) holds because of $\det(\boldsymbol{I}_p + \boldsymbol{A}\boldsymbol{B}) = \det(\boldsymbol{I}_q + \boldsymbol{B}\boldsymbol{A})$ for $\boldsymbol{A}\in\mathbb{C}^{p\times q}$ and $\boldsymbol{B}\in\mathbb{C}^{q\times p}$. It is notable that the capacity of SIMO channel given above takes a similar form to that of the MISO channel, which can be optimized by maximizing the total channel power. As a result, the alternating optimization algorithm proposed for the MISO scenario can be applied to the SIMO case as well with complexity $\mathcal{O}((L_r\gamma_r^1 + M^{2.5}\ln(1/\beta)\gamma_r^2 + ML_t + L_t\gamma_t^1)\gamma)$.

IV. Numerical Results

This section presents numerical results to assess the effectiveness of the proposed algorithms for maximizing the capacity of the MA-enabled MIMO channel. In the simulation, we consider a MIMO system with $N=4$ transmit MAs and $M=4$ receive MAs. The transmit and receive regions are set as square areas with size $A\times A$. We consider the geometry channel model, where the numbers of transmit and receive paths are the same, i.e., $L_t = L_r$. The path response matrix is assumed to be diagonal with $\boldsymbol{\Sigma}[1,1] \sim \mathcal{CN}(0, \kappa/(\kappa+1))$ and $\boldsymbol{\Sigma}[p,p] \sim \mathcal{CN}(0, 1/((\kappa+1)(L_r-1)))$ for $p=2,3,\ldots,L_r$, where κ denotes the ratio of the average power for line-of-sight (LoS) paths to that for non-line-of-sight (NLoS) paths. The elevation and azimuth AoDs/AoAs are assumed to be i.i.d. variables with the uniform distribution over $[0,\pi]$. The minimum distance between MAs is set as $D=\lambda/2$. The average SNR is defined as P/σ^2. We set convergence thresholds for the relative increment of the objective value as $\epsilon_1 = \epsilon_2 = 10^{-3}$ in Sections III-B and III-D. All the results are averaged over 4×10^4 independent channel realizations.

First, we set $L_t = L_r = 5$, $P/\sigma^2 = 5$ dB, $A = 4\lambda$, $\kappa = 1$, and show in Fig. 4 the convergence behavior of Algorithm 2 for different M and N. It is observed that the achievable rate monotonically increases and converges to a maximum value after 15 iterations for all values of M and N, which validates our analysis in Section III-D. Moreover, the converged achievable rate is increased by 48.2% as compared to that at the initial point for $M=N=2$.

Next, the performance of Algorithm 2 is compared with the following benchmark schemes:

1) **FPA**: The transmitter and receiver are equipped with FPA-based ULAs with N and M antennas, respectively, spaced by $\lambda/2$. The MIMO channel capacity is obtained according to Section III-A with fixed antenna positions.
2) **AS**: The transmitter and receiver are equipped with FPA-based ULAs with $2N$ and $2M$ antennas, respectively,

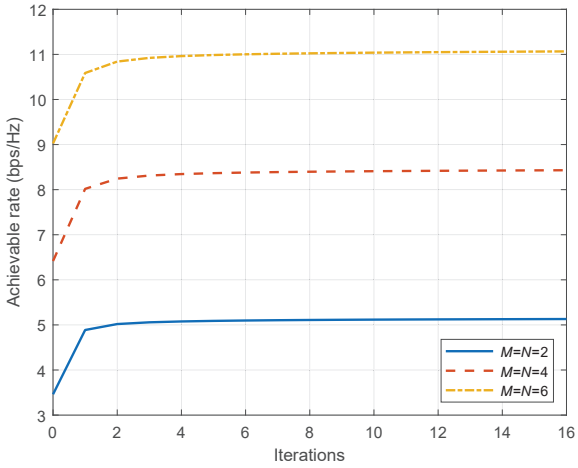

Fig. 4. Convergence behavior of Algorithm 2.

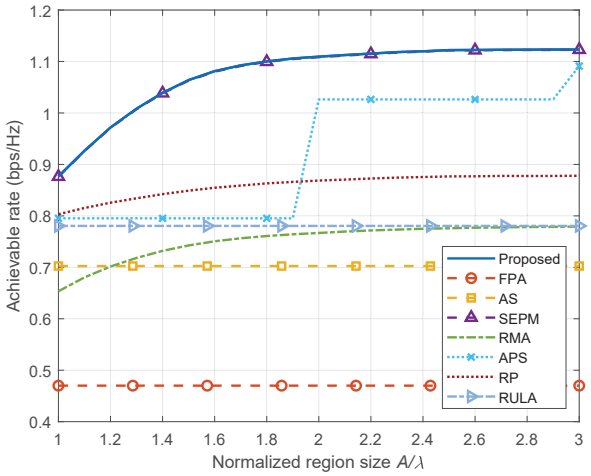

(a) Achievable rate versus normalized region size.

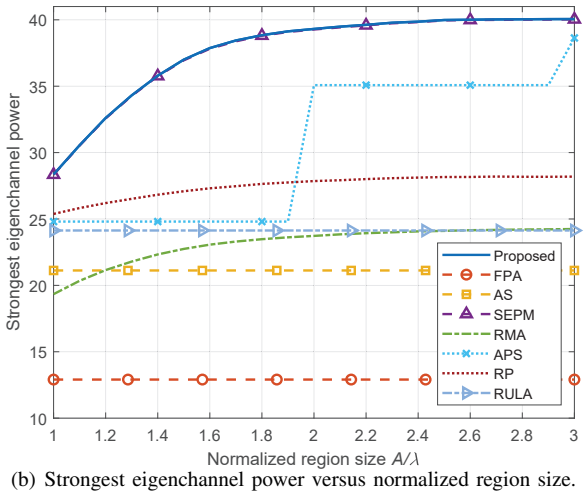

(b) Strongest eigenchannel power versus normalized region size.

Fig. 5. Performance of MA-enabled MIMO communication in the low-SNR regime.

spaced by $\lambda/2$, where N transmit antennas and M receive antennas are selected via exhaustive search to maximize the channel capacity [39].

3) **Strongest eigenchannel power maximization (SEPM)**: The simplified algorithm presented in Section III-F tailored for the low-SNR regime.
4) **Receive MA (RMA)**: The transmitter is equipped with an FPA-based ULA same as the FPA scheme, while the receiver employs M MAs [1]. Since $\{\boldsymbol{t}_n\}_{n=1}^N$ are constant with the FPA-based ULA, we only need to alternately optimize $\{\boldsymbol{r}_m\}_{m=1}^M \cup \boldsymbol{Q}$ in Algorithm 2.
5) **Alternating position selection (APS)**: The transmit/receive area is quantized into discrete locations with equal-distance $D = \lambda/2$. The proposed Algorithm 2 is applied, where problems (P2-m) and (P3-n) are solved by exhaustive search over discrete locations for each transmit/receive MA. Note that it is difficult to perform exhaustive search over all possible transmit and receive MAs' positions due to the prohibitive computational complexity. For example, considering $N = M = 4$ MAs in the $4\lambda \times 4\lambda$ transmit/receive region, the number of total channel matrices for exhaustive search is $\binom{81}{4}^2 = 2.77 \times 10^{12}$. As a result, we use Algorithm 2 to alternately select transmit and receive MA positions for lower complexity.
6) **Random position (RP)**: Randomly generate $\tilde{\boldsymbol{t}}$ and $\tilde{\boldsymbol{r}}$ satisfying (9b), (9c), (9d), and (9e) for 2500 independent realizations. Obtain the channel capacity in (8) by optimizing $\boldsymbol{Q}$ with given $\tilde{\boldsymbol{t}}$ and $\tilde{\boldsymbol{r}}$ for each realization, and select $\tilde{\boldsymbol{t}}$ and $\tilde{\boldsymbol{r}}$ with the largest capacity.
7) **RULA** [13], [14]: The transmitter and receiver are equipped with RULAs with N and M antennas, respectively, spaced by $\lambda/2$. The rotation of the transmit/receive RULA is quantized into 50 discrete angles, where the optimal transmit/receive rotated angle is selected from $50 \times 50 = 2500$ pairs to achieve the largest capacity.

We consider two SNR values of -15 dB and 25 dB corresponding to the low-SNR and high-SNR regimes, respectively. We set $L_t = L_r = 5$, $\kappa = 1$ [40]. We show the achievable rate versus the normalized region size A/λ for the proposed MA-enabled MIMO system and the benchmark schemes in Fig. 5(a) and Fig. 6(a). For both SNR regimes, it is shown that the proposed, RMA, APS and RP schemes with MAs outperform FPA systems in terms of achievable rate, and the performance gain increases with the region size. Moreover, all schemes converge when the normalized region size is larger than 4, which indicates that the maximum achievable rate of MA-enabled MIMO systems can be achieved with finite transmit and receive regions. It is also observed that our proposed algorithm achieves the best performance among all schemes in both low-SNR regime and high-SNR regime for any region size. With $P/\sigma^2 = 25$ dB and $A/\lambda = 3$, the proposed scheme achieves 29.4%, 21.4%, 55.9%, 12.3%, 2.3%, 6.9%, and 6.5% performance improvements over the FPA, AS, SEPM, RMA, APS, RP, and RULA schemes, respectively. Particularly, the proposed scheme with transmit and receive MAs outperforms the RMA scheme with only receive MAs, which shows the additional gain of jointly optimizing the transmit and receive MAs.

Furthermore, in the low-SNR regime, Fig. 5(a) shows that

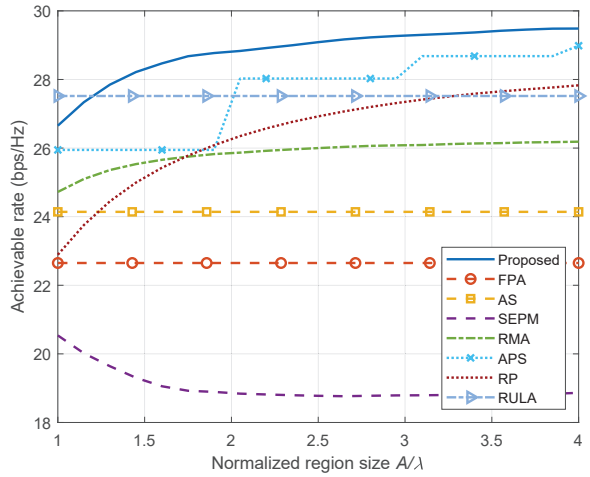

(a) Achievable rate versus normalized region size.

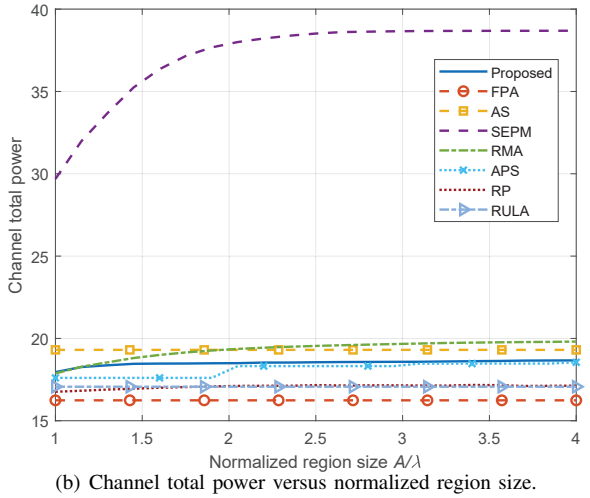

(b) Channel total power versus normalized region size.

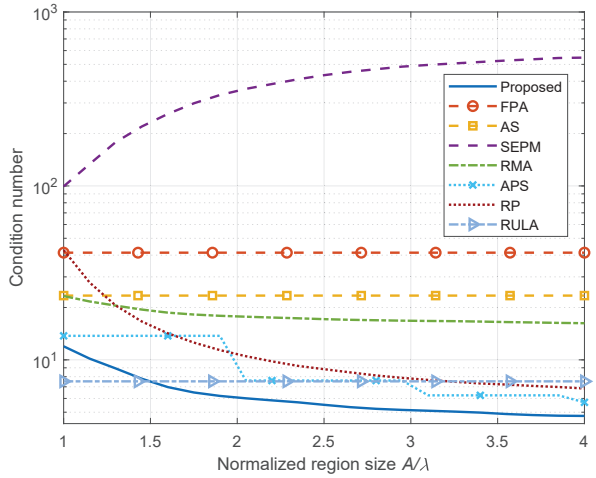

(c) Channel condition number versus normalized region size.

Fig. 6. Performance of MA-enabled MIMO communication in the high-SNR regime.

the SEPM algorithm achieves performance that is nearly identical to that of the proposed algorithm, which is consistent with the results presented in Section III-F. Thus, the SEPM scheme can be considered a low-complexity alternative to Algorithm 2 in the low-SNR regime. To gain more insight, we also present in Fig. 5(b) the average strongest eigenchannel power, $\max(\text{diag}(\tilde{\mathbf{\Lambda}}))^2$, for each scheme versus the normalized region size. It is shown that the performance gap of $\max(\text{diag}(\tilde{\mathbf{\Lambda}}))^2$ between MA and FPA schemes increases with the normalized region size. However, in the high-SNR regime shown in Fig. 6(a), the SEPM scheme achieves the lowest achievable rate. The reason is as follows. Note that the channel total power and channel condition number $\zeta = \max(\text{diag}(\tilde{\mathbf{\Lambda}}))/\min(\text{diag}(\tilde{\mathbf{\Lambda}}))$ are two important parameters influencing the MIMO channel capacity in the high-SNR regime. Generally, the channel capacity increases with the channel total power and decreases with ζ [30]. From Fig. 6(b) and Fig. 6(c), we observe that although the SEPM scheme can achieve the highest channel total power, it has the largest ζ as well. In other words, the SEPM scheme concentrates most of the channel power on the strongest eigenchannel but sacrifices the performance of the other eigenchannels, and thus the achievable rate is inferior as compared to other schemes in the high-SNR regime. It can be also observed that the channel total power of the proposed Algorithm 2 increases with the normalized region size and is higher than those of the FPA, APS, RP, and RULA schemes. Besides, the condition number of the proposed Algorithm 2 decreases with the normalized region size and is smaller than those of the FPA, AS, RMA, APS, RP, and RULA schemes. The higher channel total power and lower condition number yield more balanced power distribution over different eigenchannels of the MIMO channel, thus leading to a achievable rate gain over other schemes. The above results indicate that the proposed MA-enabled system can achieve significantly higher achievable rate over the conventional FPA-based MIMO systems by exploring more DoFs in the spatial domain via antenna position optimization, and our proposed Algorithm 2 is able to reshape the MIMO channel matrix into a more favorable condition for achievable-rate maximization.

Then, we consider a setup with $A = 3\lambda$ and two different numbers of channel paths with $L_t = L_r = 3$ and $L_t = L_r = 6$, respectively. Fig. 7 illustrates the achievable rate of the proposed and benchmark schemes versus SNR. It is shown that with the same SNR, the proposed algorithm can achieve larger achievable rate as compared to the schemes with FPAs. For the case with $P/\sigma^2 = 15$ dB and $L_t = L_r = 6$, the proposed scheme has 30.3%, 21.8%, 41.9%, 10.1%, 2.8%, 8.8%, and 7.8% performance improvements over the FPA, AS, SEPM, RMA, APS, RP, and RULA schemes, respectively. Furthermore, it is shown in Fig. 7 that our proposed and SEPM algorithms have almost the same performance when SNR is smaller than -5 dB, indicating that the SNR threshold of -5 dB guarantees that the proposed algorithm can be approximated by the SEPM scheme in the low-SNR regime. Moreover, for both two cases with different numbers of channel paths, the proposed, RMA, APS, and RP schemes yield a larger achievable rate compared to the FPA and AS schemes with FPAs, and the achievable rate gap increases with the number of channel paths. This is because the small-scale fading becomes stronger as the number of paths increases, and thus the achievable rate has more significant fluctuation in the transmit/receive region, which provides more DoFs on increasing the achievable rate for our proposed MA-enabled

This article has been accepted for publication in IEEE Transactions on Wireless Communications. This is the author's version which has not been fully edited and content may change prior to final publication. Citation information: DOI 10.1109/TWC.2023.3307696

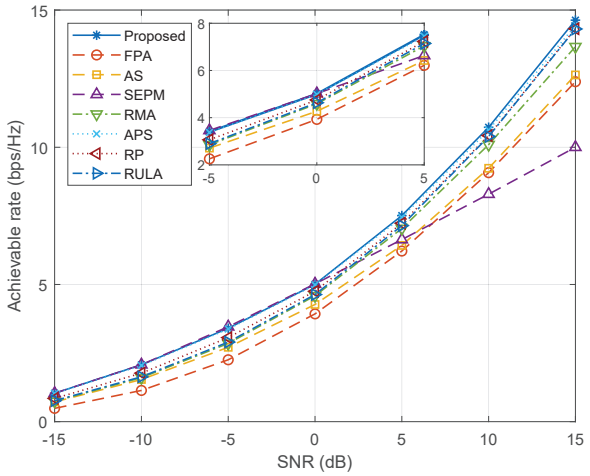

(a) $L_r = L_t = 3$.

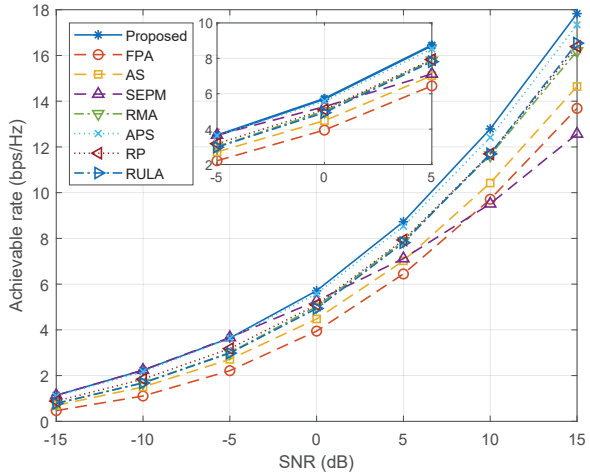

(b) $L_r = L_t = 6$.

Fig. 7. Achievable rate versus SNR for MA-enabled MIMO communication.

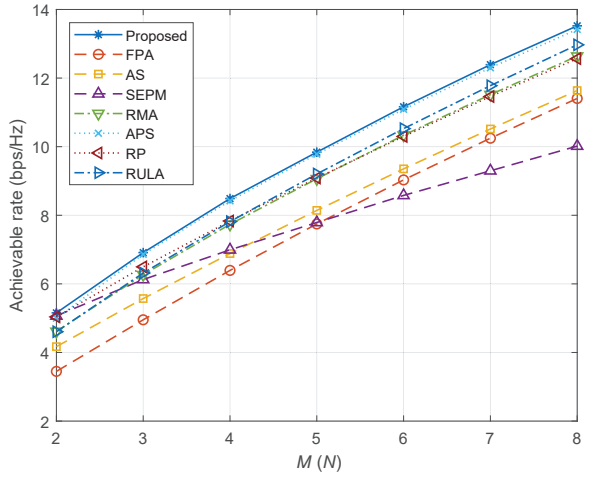

Fig. 8. Achievable rate versus $M(N)$ for MA-enabled MIMO communication.

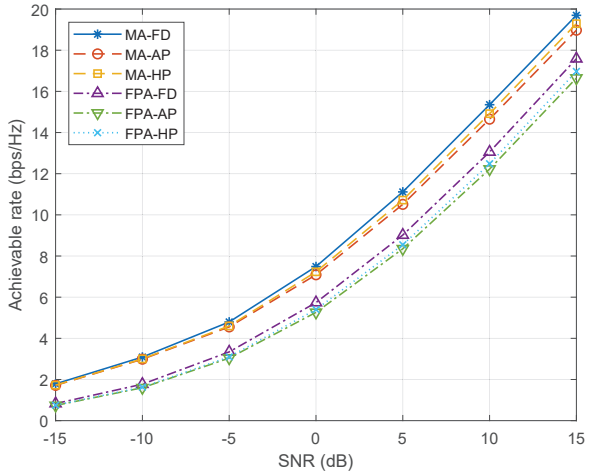

Fig. 9. Achievable rate versus SNR for different precoding/combining architectures.

MIMO systems.

Furthermore, Fig. 8 shows the achievable rate of different schemes versus $M(N)$. We set $L_t = L_r = 5$, $P/\sigma^2 = 5$ dB, $A = 4\lambda$, $\kappa = 1$, and $M = N$. Under the same $M(N)$, it is observed again that the proposed algorithm can achieve larger achievable rate as compared to the schemes with FPAs. For $M = N = 6$, the proposed scheme achieves 23.6%, 19.3%, 30.1%, 8.0%, 0.8%, 8.4%, and 6.0% performance improvements over the FPA, AS, SEPM, RMA, APS, RP, and RULA schemes, respectively. Moreover, we can see that although the number of parallel data steams is no greater than $\text{rank}(\boldsymbol{H}(\tilde{\boldsymbol{t}}, \tilde{\boldsymbol{r}})) \leq \min(L_t, L_r) = 5$, the achievable rate of the proposed algorithm increases with $M(N) > 5$. This is because the total channel power gain increases with the channel dimensions, $M(N)$, and thus larger achievable rate can be achieved with increasing $M(N)$ even for fixed-rank channels.

Finally, we show the achievable rate of the MA and FPA systems versus SNR for different precoding/combining architectures in Fig. 9. We consider the setup with $A = 4\lambda$, $L_t = L_r = 5$, $\kappa = 1$, $M = N = 6$ and $K = 3$ RF chains. We consider three precoding/combining architectures: i) **FD**: let $\overline{\boldsymbol{V}} \in \mathbb{C}^{N\times K}$ and $\overline{\boldsymbol{U}} \in \mathbb{C}^{M\times K}$ denote the first K columns of $\tilde{\boldsymbol{V}}$ and $\tilde{\boldsymbol{U}}$, respectively. Define $\overline{\boldsymbol{P}} \triangleq \text{diag}([\sqrt{p_1^\star}, \sqrt{p_2^\star}, \ldots, \sqrt{p_K^\star}]) \in \mathbb{C}^{K\times K}$. Then, the digital transmit precoding matrix and receive combining matrix are set as $\boldsymbol{T}^\star = \overline{\boldsymbol{V}}\overline{\boldsymbol{P}} \in \mathbb{C}^{N\times K}$ and $\boldsymbol{R}^\star = \overline{\boldsymbol{U}} \in \mathbb{C}^{M\times K}$, respectively. ii) **AP** [9]: the transmitter employs a diagonal power allocation matrix and an AP matrix, resulting in the equivalent precoding matrix as $e^{j\angle\overline{\boldsymbol{V}}}\overline{\boldsymbol{P}}/\sqrt{N}$; and the receiver employs an analog combining matrix as $e^{j\angle\overline{\boldsymbol{U}}^H}$. iii) **HP** [10]: the transmitter employs an AP matrix $\boldsymbol{T}_{RF} = e^{j\angle\boldsymbol{T}^\star}$ and a digital precoding matrix $\boldsymbol{T}_{BB} = \sqrt{P}\boldsymbol{T}_{RF}^\dagger\boldsymbol{T}^\star/\|\boldsymbol{T}_{RF}\boldsymbol{T}_{RF}^\dagger\boldsymbol{T}^\star\|_F$; and the receiver employs an analog combining matrix $\boldsymbol{R}_{RF} = e^{j\angle\boldsymbol{R}^\star}$ and a digital combining matrix $\boldsymbol{R}_{BB} = \boldsymbol{R}^\star\boldsymbol{R}_{RF}^\dagger$. The equivalent transmit precoding matrix and receive combining matrix are $\boldsymbol{T}_{RF}\boldsymbol{T}_{BB}$ and $\boldsymbol{R}_{BB}\boldsymbol{R}_{RF}$, respectively. As shown in Fig. 9, for all precoding/combining architectures, the proposed scheme with MAs outperforms FPA systems in terms of achievable rate. For $P/\sigma^2 = 5$ dB, the achievable rate of the MA-AP system is increased by 16.5%, 25.8%, and 23.0% as compared to that of the FPA-FD, FPA-AP, and FPA-HP systems, respectively. Therefore, MAs can be equipped in

HP/AP architectures to reduce the RF chain cost, while higher achievable rate can be achieved compared to the FPA systems.

V. Conclusions

In this paper, we proposed a new MA-enabled MIMO system to increase the channel capacity by exploiting the antenna position optimization at the transmitter and receiver. We studied the capacity maximization problem for MA-enabled point-to-point MIMO communication, via the joint optimization of the transmit and receive MA positions as well as transmit covariance matrix. An alternating optimization algorithm was proposed to find a locally optimal solution by iteratively optimizing the position of each transmit/receive MA and the transmit covariance matrix with the other variables being fixed. Moreover, alternative algorithms of lower complexity were also proposed for the asymptotically low-SNR regime as well as MISO/SIMO channels. Numerical results showed that our proposed system and algorithm achieve significantly higher capacity over the conventional FPAs-based MIMO systems with/without AS in multi-path environment, especially when the transmit/receive region is sufficiently large. Moreover, it was revealed that by jointly optimizing transmit and receive MA positions, the MIMO channel power can be significantly improved while the condition number of the MIMO channel decreases, thus leading to more favorable MIMO channel realizations for enhancing the capacity.

Appendix

A. Derivations of $\nabla\bar{g}(\boldsymbol{r}_m)$ and $\nabla^2\bar{g}(\boldsymbol{r}_m)$

For ease of exposition, we define

$$\boldsymbol{b} \triangleq \boldsymbol{B}_m \boldsymbol{f}(\boldsymbol{r}_m^i) \in \mathbb{C}^{L_r}. \tag{38}$$

Further denote the qth entry of $\boldsymbol{b}$ as $b_q = |b_q| e^{j\angle b_q}$, with amplitude $|b_q|$ and phase $\angle b_q$. Thus, $\bar{g}(\boldsymbol{r}_m)$ can be written as

$$\begin{aligned}\bar{g}(\boldsymbol{r}_m) &= \mathrm{Re}\left\{\boldsymbol{b}^H \boldsymbol{f}(\boldsymbol{r}_m)\right\} \qquad (39)\\ &= \mathrm{Re}\left\{\sum_{q=1}^{L_r} |b_q| e^{j\left(\frac{2\pi}{\lambda}(x_{r,m}\sin\theta_r^q\cos\phi_r^q + y_{r,m}\cos\theta_r^q) - \angle b_q\right)}\right\}\\ &= \sum_{q=1}^{L_r} |b_q| \cos\left(\kappa^q(\boldsymbol{r}_m)\right),\end{aligned}$$

with $\kappa^q(\boldsymbol{r}_m) \triangleq 2\pi\rho_r^q(\boldsymbol{r}_m)/\lambda - \angle b_q$. Recalling that $\boldsymbol{r}_m = [x_{r,m}, y_{r,m}]^T$, the gradient vector and Hessian matrix of $\bar{g}(\boldsymbol{r}_m)$ over $\boldsymbol{r}_m$ can be represented as $\nabla\bar{g}(\boldsymbol{r}_m) = \left[\frac{\partial\bar{g}(\boldsymbol{r}_m)}{\partial x_{r,m}}, \frac{\partial\bar{g}(\boldsymbol{r}_m)}{\partial y_{r,m}}\right]^T$ and $\nabla^2\bar{g}(\boldsymbol{r}_m) = \begin{bmatrix} \frac{\partial\bar{g}(\boldsymbol{r}_m)}{\partial x_{r,m}\partial x_{r,m}} & \frac{\partial\bar{g}(\boldsymbol{r}_m)}{\partial x_{r,m}\partial y_{r,m}} \\ \frac{\partial\bar{g}(\boldsymbol{r}_m)}{\partial y_{r,m}\partial x_{r,m}} & \frac{\partial\bar{g}(\boldsymbol{r}_m)}{\partial y_{r,m}\partial y_{r,m}} \end{bmatrix}$, respectively. Thus, we have

$$\begin{aligned}\frac{\partial\bar{g}(\boldsymbol{r}_m)}{\partial x_m} &= -\frac{2\pi}{\lambda}\sum_{q=1}^{L_r} |b_q| \sin\theta_r^q \cos\phi_r^q \sin\left(\kappa^q(\boldsymbol{r}_m)\right),\\ \frac{\partial\bar{g}(\boldsymbol{r}_m)}{\partial y_m} &= -\frac{2\pi}{\lambda}\sum_{q=1}^{L_r} |b_q| \cos\theta_r^q \sin\left(\kappa^q(\boldsymbol{r}_m)\right), \qquad (40)\end{aligned}$$

and

$$\begin{aligned}\frac{\partial\bar{g}(\boldsymbol{r}_m)}{\partial x_m\partial x_m} &= -\frac{4\pi^2}{\lambda^2}\sum_{q=1}^{L_r} |b_q| \sin^2\theta_r^q \cos^2\phi_r^q \cos\left(\kappa^q(\boldsymbol{r}_m)\right),\\ \frac{\partial\bar{g}(\boldsymbol{r}_m)}{\partial x_m\partial y_m} &= -\frac{4\pi^2}{\lambda^2}\sum_{q=1}^{L_r} |b_q| \sin\theta_r^q \cos\phi_r^q \cos\theta_r^q \cos\left(\kappa^q(\boldsymbol{r}_m)\right),\\ \frac{\partial\bar{g}(\boldsymbol{r}_m)}{\partial y_m\partial x_m} &= -\frac{4\pi^2}{\lambda^2}\sum_{q=1}^{L_r} |b_q| \sin\theta_r^q \cos\phi_r^q \cos\theta_r^q \cos\left(\kappa^q(\boldsymbol{r}_m)\right),\\ \frac{\partial\bar{g}(\boldsymbol{r}_m)}{\partial y_m\partial y_m} &= -\frac{4\pi^2}{\lambda^2}\sum_{q=1}^{L_r} |b_q| \cos^2\theta_r^q \cos\left(\kappa^q(\boldsymbol{r}_m)\right). \qquad (41)\end{aligned}$$

B. Construction of δ_m

Based on the definition of $\nabla^2\bar{g}(\boldsymbol{r}_m)$ in Appendix A, we have

$$\begin{aligned}\|\nabla^2\bar{g}(\boldsymbol{r}_m)\|_2^2 &\le \|\nabla^2\bar{g}(\boldsymbol{r}_m)\|_F^2 \qquad (42)\\ &= \left(\frac{\partial\bar{g}(\boldsymbol{r}_m)}{\partial x_{r,m}\partial x_{r,m}}\right)^2 + \left(\frac{\partial\bar{g}(\boldsymbol{r}_m)}{\partial x_{r,m}\partial y_{r,m}}\right)^2\\ &\quad + \left(\frac{\partial\bar{g}(\boldsymbol{r}_m)}{\partial y_{r,m}\partial x_{r,m}}\right)^2 + \left(\frac{\partial\bar{g}(\boldsymbol{r}_m)}{\partial y_{r,m}\partial y_{r,m}}\right)^2\\ &\le 4\left(\frac{4\pi^2}{\lambda^2}\sum_{q=1}^{L_r}|b_q|\right)^2.\end{aligned}$$

Since $\|\nabla^2\bar{g}(\boldsymbol{r}_m)\|_2\boldsymbol{I}_2 \succeq \nabla^2\bar{g}(\boldsymbol{r}_m)$, we can select δ_m as

$$\delta_m = \frac{8\pi^2}{\lambda^2}\sum_{q=1}^{L_r}|b_q|, \tag{43}$$

satisfying $\delta_m \ge \|\nabla^2\bar{g}(\boldsymbol{r}_m)\|_2$, and thus we have $\delta_m\boldsymbol{I}_2 \succeq \nabla^2\bar{g}(\boldsymbol{r}_m)$.

References

[1] W. Ma, L. Zhu, and R. Zhang, "Capacity maximization for movable antenna enabled MIMO communication," in *Proc. IEEE ICC*, Rome, Italy, 2023.

[2] W. Jiang, B. Han, M. A. Habibi, and H. D. Schotten, "The road towards 6G: A comprehensive survey," *IEEE Open J. Commun. Soc.*, vol. 2, pp. 334–366, Feb. 2021.

[3] W. Saad, M. Bennis, and M. Chen, "A vision of 6G wireless systems: Applications, trends, technologies, and open research problems," *IEEE Netw.*, vol. 34, no. 3, pp. 134–142, May 2020.

[4] M. Z. Chowdhury, M. Shahjalal, S. Ahmed, and Y. M. Jang, "6G wireless communication systems: Applications, requirements, technologies, challenges, and research directions," *IEEE Open J. Commun. Soc.*, vol. 1, pp. 957–975, 2020.

[5] L. Zhu, J. Zhang, Z. Xiao, X. Cao, D. O. Wu, and X. Xia, "Millimeter-wave NOMA with user grouping, power allocation and hybrid beamforming," *IEEE Trans. Wireless Commun.*, vol. 18, no. 11, pp. 5065–5079, Nov. 2019.

[6] L. Lu, G. Y. Li, A. L. Swindlehurst, A. Ashikhmin, and R. Zhang, "An overview of massive MIMO: Benefits and challenges," *IEEE J. Sel. Topics Signal Process.*, vol. 8, no. 5, pp. 742–758, Oct. 2014.

[7] S. Sanayei and A. Nosratinia, "Antenna selection in MIMO systems," *IEEE Commun. Mag.*, vol. 42, no. 10, pp. 68–73, Oct. 2004.

[8] M. Gharavi-Alkhansari and A. B. Gershman, "Fast antenna subset selection in MIMO systems," *IEEE Trans. Signal Process.*, vol. 52, no. 2, pp. 339–347, Feb. 2004.

[9] X. Zhang, A. F. Molisch, and S.-Y. Kung, "Variable-phase-shift-based RF-baseband codesign for MIMO antenna selection," *IEEE Trans. Signal Process.*, vol. 53, no. 11, pp. 4091–4103, Nov. 2005.

[10] A. Kaushik, J. Thompson, E. Vlachos, C. Tsinos, and S. Chatzinotas, "Dynamic RF chain selection for energy efficient and low complexity hybrid beamforming in millimeter wave MIMO systems," *IEEE Trans. Green Commun. Netw.*, vol. 3, no. 4, pp. 886–900, Jul. 2019.

[11] Y. Teng, Y. Zhao, M. Wei, A. Liu, and V. K. Lau, "Sparse hybrid precoding for power minimization with an adaptive antenna structure in massive MIMO systems," *IEEE Trans. Wireless Commun.*, vol. 21, no. 7, pp. 5279–5292, Jul. 2022.

[12] X. Zhu, Z. Wang, L. Dai, and Q. Wang, "Adaptive hybrid precoding for multiuser massive MIMO," *IEEE Commun. Lett.*, vol. 20, no. 4, pp. 776–779, Apr. 2016.

[13] H. Do, N. Lee, and A. Lozano, "Reconfigurable ULAs for line-of-sight MIMO transmission," *IEEE Trans. Wireless Commun.*, vol. 20, no. 5, pp. 2933–2947, May 2021.

[14] H. Do, S. Cho, J. Park, H.-J. Song, N. Lee, and A. Lozano, "Terahertz line-of-sight MIMO communication: Theory and practical challenges," *IEEE Commun. Magazine*, vol. 59, no. 3, pp. 104–109, Mar. 2021.

[15] K.-K. Wong, A. Shojaeifard, K.-F. Tong, and Y. Zhang, "Fluid antenna systems," *IEEE Trans. Wireless Commun.*, vol. 20, no. 3, pp. 1950–1962, Mar. 2021.

[16] K.-K. Wong and K.-F. Tong, "Fluid antenna multiple access," *IEEE Trans. Wireless Commun.*, vol. 21, no. 7, pp. 4801–4815, Jul. 2022.

[17] Z. Zhang and L. Dai, "Pattern-division multiplexing for continuous-aperture MIMO," in *Proc. IEEE ICC*, Seoul, Korea, Republic of, May 2022, pp. 1–6.

[18] C. Huang, S. Hu, G. C. Alexandropoulos, A. Zappone, C. Yuen, R. Zhang, M. D. Renzo, and M. Debbah, "Holographic MIMO surfaces for 6G wireless networks: Opportunities, challenges, and trends," *IEEE Trans. Wireless Commun.*, vol. 27, no. 5, pp. 118–125, Oct. 2020.

[19] A. Pizzo, L. Sanguinetti, and T. L. Marzetta, "Fourier plane-wave series expansion for holographic MIMO communications," *IEEE Trans. Wireless Commun.*, vol. 21, no. 9, pp. 6890–6905, Sep. 2022.

[20] N. Decarli and D. Dardari, "Communication modes with large intelligent surfaces in the near field," *IEEE Access*, vol. 9, pp. 165 648–165 666, Dec. 2021.

[21] R. Deng, B. Di, H. Zhang, Y. Tan, and L. Song, "Reconfigurable holographic surface: Holographic beamforming for metasurface-aided wireless communications," *IEEE Trans. Veh. Technol.*, vol. 70, no. 6, pp. 6255–6259, Jun. 2021.

[22] L. Wei, C. Huang, G. Alexandropoulus, W. E. Sha, Z. Zhang, M. Debbah, and C. Yuen, "Multi-user holographic MIMO surfaces: Channel modeling and spectral efficiency analysis," *IEEE J. Sel. Top. Signal Process.*, vol. 16, no. 5, pp. 1112–1124, Aug. 2022.

[23] T. Ismail and M. Dawoud, "Null steering in phased arrays by controlling the elements positions," *IEEE Trans. Antennas Propagat.*, vol. 39, no. 11, pp. 1561–1566, Nov. 1991.

[24] S. Basbug, "Design and synthesis of antenna array with movable elements along semicircular paths," *IEEE Antennas Wireless Propag. Lett.*, vol. 16, pp. 3059–3062, Oct. 2017.

[25] A. Zhuravlev, V. Razevig, S. Ivashov, A. Bugaev, and M. Chizh, "Experimental simulation of multi-static radar with a pair of separated movable antennas," in *Proc. IEEE COMCAS*, Tel Aviv, Israel, Nov. 2015, pp. 1–5.

[26] L. Zhu, W. Ma, and R. Zhang, "Movable antennas for wireless communication: Opportunities and challenges," *arXiv preprint arXiv:2306.02331*, 2023.

[27] ——, "Modeling and performance analysis for movable antenna enabled wireless communications," *arXiv preprint arXiv:2210.05325*, 2022.

[28] L. Zhu, W. Ma, B. Ning, and R. Zhang, "Movable-antenna enhanced multiuser communication via antenna position optimization," *arXiv preprint arXiv:2302.06978*, 2023.

[29] W. Ma, L. Zhu, and R. Zhang, "Compressed sensing based channel estimation for movable antenna communications," *arXiv preprint arXiv:2306.04333*, 2023.

[30] A. Goldsmith, *Wireless Communications*. Cambridge, U.K.: Cambridge Univ. Press, 2005.

[31] K. B. Petersen and M. S. Pedersen, *The Matrix Cookbook*. Kgs. Lyngby, Denmark: Tech. Univ. Denmark, 2006.

[32] Q. Wu, Y. Zeng, and R. Zhang, "Joint trajectory and communication design for multi-UAV enabled wireless networks," *IEEE Trans. Wireless Commun.*, vol. 17, no. 3, pp. 2109–2121, Mar. 2018.

[33] J. R. Magnus and H. Neudecker, *Matrix Differential Calculus With Applications in Statistics and Econometrics*. Hoboken, NJ, USA: Wiley, 1995.

[34] B. A. Turlach and A. Weingessel, "quadprog: Functions to solve quadratic programming problems," *CRAN-Package quadprog*, 2007.

[35] A. Ben-Tal and A. Nemirovski, *Lectures on Modern Convex Optimization: Analysis, Algorithms and Engineering Applications*. Philadelphia, PA, USA: SIAM, 2001.

[36] S. Zhang and R. Zhang, "Capacity characterization for intelligent reflecting surface aided MIMO communication," *IEEE J. Sel. Areas Commun.*, vol. 38, no. 8, pp. 1823–1838, Aug. 2020.

[37] *Packings of Equal Circles in Fixed-Sized Containers with Maximum Packing Density*, Accessed: Apr. 5, 2017. [Online]. Available: http://www.packomania.com.

[38] M. Fu, Y. Zhou, Y. Shi, W. Chen, and R. Zhang, "UAV aided over-the-air computation," *IEEE Trans. Wireless Commun.*, vol. 21, no. 7, pp. 4909–4924, Jul. 2022.

[39] S. Sanayei and A. Nosratinia, "Capacity maximizing algorithms for joint transmit–receive antenna selection," in *Proc. IEEE ACSSC*, Pacific Grove, CA, USA, Nov. 2004, pp. 1773–1776.

[40] 3GPP, "Study on channel model for frequency spectrum above 6 GHz," *3rd Generation Partnership Project (3GPP), TR 38.900 V14.2.0*, Dec. 2016.

Wenyan Ma (Student Member, IEEE) (S'17) received the B.S. degree (Hons.) in information engineering and the M.S. degree in signal and information processing from the Southeast University, Nanjing, China, in 2017 and 2020, respectively. He is currently pursuing the Ph.D. degree with the Department of Electrical and Computer Engineering, National University of Singapore. His research interests include movable antenna (MA)-enabled wireless communications, intelligent reflecting surface, and convex optimization. He was the recipient of the Outstanding Master's Thesis Award from the Chinese Institute of Electronics in 2020, and the Best Paper Award from the Eleventh International Conference on Wireless Communications and Signal Processing in 2019. He was honored as the Exemplary Reviewer of the IEEE COMMUNICATIONS LETTERS in 2019 and 2020.

Lipeng Zhu (Member, IEEE) received the B.S. degree in the Department of Mathematics and System Sciences from Beihang University in 2017, and the Ph.D. degree in the Department of Electronic and Information Engineering from Beihang University in 2021. He is currently a Research Fellow with the Department of Electrical and Computer Engineering, National University of Singapore. His current research interests include movable antenna (MA)-enabled wireless communications, intelligent reflecting surface (IRS), millimeter-wave communications, unmanned aerial vehicle (UAV) communications, and non-orthogonal multiple access (NOMA). He was a recipient of the Best Ph.D. Thesis Award from China Education Society of Electronics in 2022, the Best Ph.D. Thesis Award of Beijing in 2022, and the First Prize of Natural Science from Chinese Institute of Electronics. He served as a guest editor for China Communications. He was also a recipient of the Exemplary Reviewer of the IEEE Transactions on Communications.

Rui Zhang (Fellow, IEEE) (S'00-M'07-SM'15-F'17) received the B.Eng. (first-class Hons.) and M.Eng. degrees from the National University of Singapore, Singapore, and the Ph.D. degree from the Stanford University, Stanford, CA, USA, all in electrical engineering.

From 2007 to 2009, he worked as a researcher at the Institute for Infocomm Research, ASTAR, Singapore. In 2010, he joined the Department of Electrical and Computer Engineering of National University of Singapore, where he was appointed as a Provost's Chair Professor in 2020. Since 2022, he has joined the School of Science and Engineering, The Chinese University of Hong Kong, Shenzhen, as a Principal's Diligence Chair Professor. He has published over 300 journal papers and over 200 conference papers. He has been listed as a Highly Cited Researcher by Thomson Reuters/Clarivate Analytics since 2015. His current research interests include UAV/satellite communications, wireless power transfer, intelligent reflecting surface, reconfigurable MIMO, radio mapping and optimization methods.

He was the recipient of the 6th IEEE Communications Society Asia-Pacific Region Best Young Researcher Award in 2011, the Young Researcher Award of National University of Singapore in 2015, the Wireless Communications Technical Committee Recognition Award in 2020, and the IEEE Signal Processing and Computing for Communications (SPCC) Technical Recognition Award in 2020. He received 14 IEEE Best Paper Awards, including the IEEE Marconi Prize Paper Award in Wireless Communications in 2015 and 2020, the IEEE Signal Processing Society Best Paper Award in 2016, the IEEE Communications Society Heinrich Hertz Prize Paper Award in 2017, 2020 and 2022, the IEEE Communications Society Stephen O. Rice Prize in 2021, etc. He served for over 30 international conferences as the TPC co-chair or an organizing committee member. He was an elected member of the IEEE Signal Processing Society SPCOM Technical Committee from 2012 to 2017 and SAM Technical Committee from 2013 to 2015, and served as the Vice Chair of the IEEE Communications Society Asia-Pacific Board Technical Affairs Committee from 2014 to 2015. He was a Distinguished Lecturer of IEEE Signal Processing Society and IEEE Communications Society from 2019 to 2020. He served as an Editor for the IEEE TRANSACTIONS ON WIRELESS COMMUNICATIONS from 2012 to 2016, the IEEE JOURNAL ON SELECTED AREAS IN COMMUNICATIONS: Green Communications and Networking Series from 2015 to 2016, the IEEE TRANSACTIONS ON SIGNAL PROCESSING from 2013 to 2017, the IEEE TRANSACTIONS ON GREEN COMMUNICATIONS AND NETWORKING from 2016 to 2020, and the IEEE TRANSACTIONS ON COMMUNICATIONS from 2017 to 2022. He served as a member of the Steering Committee of the IEEE Wireless Communications Letters from 2018 to 2021. He is a Fellow of the Academy of Engineering Singapore.